energies

MDPI

Article

Wind Turbine Driving a PM Synchronous Generator Using Novel Recurrent Chebyshev Neural Network Control with the Ideal Learning Rate

Chih-Hong Lin

Department of Electrical Engineering, National Uinted University, Miaoli 36063, Taiwan; jhlin@nuu.edu.tw; Tel.: +886-3-738-2464; Fax: +886-3-738-2488

Academic Editor: Frede Blaabjerg
Received: 4 March 2016; Accepted: 3 June 2016; Published: 9 June 2016

Abstract: A permanent magnet (PM) synchronous generator system driven by wind turbine (WT), connected with smart grid via AC-DC converter and DC-AC converter, are controlled by the novel recurrent Chebyshev neural network (NN) and amended particle swarm optimization (PSO) to regulate output power and output voltage in two power converters in this study. Because a PM synchronous generator system driven by WT is an unknown non-linear and time-varying dynamic system, the on-line training novel recurrent Chebyshev NN control system is developed to regulate DC voltage of the AC-DC converter and AC voltage of the DC-AC converter connected with smart grid. Furthermore, the variable learning rate of the novel recurrent Chebyshev NN is regulated according to discrete-type Lyapunov function for improving the control performance and enhancing convergent speed. Finally, some experimental results are shown to verify the effectiveness of the proposed control method for a WT driving a PM synchronous generator system in smart grid.

Keywords: permanent magnet synchronous generator; wind turbine; recurrent Chebyshev neural network; discrete-type Lyapunov function

1. Introduction

Clean energy sources such as wind, photovoltaic, and fuel cells can be interfaced to a multi-level converter system for high power applications [1–3]. The permanent magnet (PM) synchronous generator system has been used for a wind power generating system due to simpler structure, better reliability *etc.* [4–8]. The output behavior of a wind turbine is a nonlinear and time-varying system. Thus, the control of operating point is indispensable for maximum output power. The AC-DC converter is used to convert varied AC voltage generated by PM synchronous generator into DC voltage. Then, the DC-AC converter is used to convert DC voltage into AC voltage with fixed frequency in order to provide for the smart grid of utilization. Wind turbines (WTs) are rotating machines that can be used to generate electricity from the kinetic power of the wind. WTs can deliver appropriate energy to smart grid power via the power conveter. According to these purposes, the better structure for a power conversion in wind turbines is the AC-DC-AC power converter [9,10].

Over the past decade, many different control approaches were used for generators and WT for energy generation [11–15]. In [11], a fuzzy logic control is adopted to control the power of the wind electrical conversion system transmitted to the grid and generator speed. The advantage in using a fuzzy logic controller *versus* a standard proportional-integral (PI) controller, is pointed out in better response to frequently changes in wind speed. In [12], the rule-based fuzzy-logic based maximum power point tracking (MPPT) strategy is proposed for PM synchronous generator variable speed wind turbine generation systems. The fuzzy-logic-based output power smoothing method of a wind energy conversion system (WECS) with a PM synchronous generator using the inertia of WT was proposed

in [13]. In [14], a sliding mode control (SMC) strategy associated with the field-oriented control of a dual stator induction generator (DSIG) based wind energy conversion systems was proposed to control the output power of a DSIG. In [15], a fuzzy logic sliding mode loss-minimization control is adopted to control the speed of the PM synchronous generator, and PI controller is adopted to control the WT pitch angle. However, most of these approaches require the time-consuming trial-and-error tuning procedure to achieve satisfactory performance; some of them can not achieve satisfactory performance; and some of them do not possess online learning ability and given the stability analysis. Therefore, many neural network (NNs) control approaches were used for controlling the generator and WT systems for energy generation [16–18]. In [16], a radial basis function neural network (RBFNN) control is adopted to control the PM synchronous generator on variable speed WT generation system, and to control the WT pitch angle. In [17], a new Elman NN control is adopted to control the PM synchronous generator, and to regulate the adjustable-pitch variable-speed wind-energy conversion systems. In [18], a recurrent modified Elman neural network control (RMENN) control is adopted to control the PM synchronous generator using a WT emulator system. However, these NNs have also slower convergence speed due to adopted fixed learning rates of parameters in these recurrent NNs. Therefore, in order to reduce network complexity and speed-up convergence, the novel simpler NN structure of novel recurrent Chebyshev NN, which has not only self feedback connection in the Chebyshev layer but also recurrent connection between the output layer and the input layer, is more powerful than the recurrent NN for dealing with time-varying and nonlinear dynamic system, and the optimal learning rate of parameters in the novel recurrent Chebyshev NN are proposed to enhance convergence speed in this paper.

2. Literature Review

Artificial neural networks (NNs) have emerged as a powerful learning technique to perform complex tasks in highly nonlinear dynamic systems and controls [19–21]. Some of the prime advantages of using NN are: their ability to learn based on optimization of an appropriate error function and their excellent performance for approximation of nonlinear functions. One of the major drawbacks of the NN is that it is computationally intensive and needs large number of iterations for its training. In order to reduce the computational complexity, a functional-link NN, which shown that it is capable of producing similar performance as that of NN but with much less computational cost, is shown in [22,23]. Moreover, a functional-link NN-based nonlinear dynamic system identification with satisfactory results has been reported in [24]. It is shown that the performance of functional-link NN is similar to that of a NN but with faster convergence and lesser computational complexity. Moreover, a comprehensive survey on various applications of functional-link NN has been proposed in [25].

Namatame *et al.* [26] first developed Pattern classification using Chebyshev NN. Li *et al.* [27] proposed Chebyshev polynomial-based unified model NN for static function approximation. It is based on a functional link NN with Chebyshev polynomial expansion in which recursive least square learning algorithm is used. It is pointed out that this network has universal approximation capability and has faster convergence than the multilayer feedforward NN. One of the solutions for the problem of slow convergence of multilayer feedforward NN is to use some efficient learning algorithm instead of the Backpropagation (BP) algorithm. In this direction, the scaled complex conjugate gradient algorithm as proposed by Moeller [28] is of great importance. This algorithm chooses the search direction and the step size using information from a second order Taylor expansion of the error function. Some of the other proposals on higher order conjugate gradient algorithms are presented [29–31]. Madyastha *et al.* [32] proposed multilayer feedforward NN trained by conjugate gradient algorithm to solve data classification and function interpolation problems.

The recurrent NN has received increasing attention due to its structural advantage in nonlinear system modeling and dynamic system control [33,34]. In the general recurrent NN, the specific self-connection feedback of the hidden neuron or output neuron is responsible for memorizing the specific previous activation of the hidden neuron or output neuron and feed to itself only. Therefore,

the outputs of the other neurons have no ability to affect the specific neuron. If each neuron in the recurrent NN is considered as a state in the nonlinear dynamic systems, the self-connection feedback type is unable to approximate the dynamic systems efficiently. On the other hand, the feedbacks in the recurrent Chebyshev NN not only are self-connecting but they also store in the hidden neurons and feed to all the Chebyshev neurons. Hence, the recurrent Chebyshev NN, which proved to have more advantages than the basic Chebyshev NN including a better dynamic performance, a higher accuracy and a fast transient performance, is more powerful than the general recurrent NN for dealing with time-varying and nonlinear dynamic systems. The proposed novel recurrent Chebyshev NN in this study can be considered to be a special type of recurrent NN with feedback connections from the Chebyshev layer to the function layer. The function layer is an additional layer that is used as an extra memory to memorize previous activations of the hidden neurons and feed to all the hidden neurons after the one-step time delay. Therefore, compared with the general recurrent NNs [33,34], the proposed novel recurrent Chebyshev NN has a special explicit memory to store the temporal information. Due to the function neurons, it has certain dynamical advantages over static NN [19–21] and it also has been widely applied in dynamical systems' identification and control [26–32].

Since the PM synchronous generators have a robust construction, and lower initial and lower maintenance costs, they are suitable for application to smart grid power applications. Due to nonlinear dynamics of PM synchronous generators using a WT system [12–18], the recurrent NN controller may not provide satisfactory control performance. Therefore, the novel recurrent Chebyshev NN control system for a WT driving a PM synchronous generator system is proposed to regulate both the DC bus voltage of the rectifier and the AC 60 Hz line voltage of the inverter in this study. In addition, since this study is dealing with an isolated system with maximum power control, the exceeding power must be consumed to yield system power balance. The more realistic way of control is to choose the DC voltage as the controlled variable. Moreover, if the controlled plant has highly nonlinear uncertainties, the PI and PID controllers may also not provide satisfactory control performance. Therefore, both DC voltage control of the AC-DC converter and AC voltage of the DC-AC converter using the two sets of novel recurrent Chebyshev NN control systems are implemented in this paper. The on-line adaptive laws are derived based on the Lyapunov stability theorem so that the stability of the system can be guaranteed. An on-line training methodology with variable learning rate for the novel recurrent Chebyshev NN control system is proposed in this study. Finally, to demonstrate better dynamic characteristics of the proposed novel recurrent Chebyshev NN control system, comparative studies with the PI controller and the conventional NN controller are demonstrated by experimental results. The control performance of the proposed novel recurrent Chebyshev NN control system is much improved and can be verified by some experimental results.

3. Description of a Wind Turbine Driving a PM Synchronous Generator System

The variable speed WT driving a PM synchronous generator system can be described as follows:

3.1. Model of WT System

Two characteristic curves of the wind power *versus* rotor speed for WT with three-blade horizontal axis type at different wind speeds in steady state are shown in Figures 1 and 2. According to aerodynamic principle [1,4–7], the tip speed ratio β of the WT can be expressed as:

$$\beta = R_1 \, \omega_{r1} / v_1 \tag{1}$$

where β is the tip speed ratio of the WT, R_1 is the rotor radius of the WT in meter, ω_{r1} is the rotor speed of the WT in rad/s, and v_1 is the wind speed in m/s. The output mechanical power P_1 of the WT can be expressed as [1,4–7]

$$P_1 = \rho_1 A_1 D_p(\beta) v_1^3/2 = \rho_1 A_1 D_p(\beta) R_1^3 \omega_{r1}^3/(2\beta^3) \tag{2}$$

where ρ_1 is the density of air in kg/m^3 and A_1 is the undraped area in m^2. The generated torque of the WT for different wind speeds can be obtained from the $D_p(\beta) - \beta$ curve in modeling usage. The maximum aerodynamic efficiency can result from the optimum tip speed ratio shown in Figures 1 and 2. In low speed blade turbines with more than two blades, the power coefficient varies between 0.2 and 0.5 [4–7]. The produced torque of the WT can be expressed as [1,4–7]:

$$T_1 = P_1/\omega_{r1} = \rho_1 A_1 R_1^3 D_p(\beta)\omega_{r1}^2/(2\beta^3) \quad (3)$$

where T_1 is the produced torque of the WT in Nm. The dynamic equation of torque, can be expressed as:

$$T_1 - T_{e1} = J_1 \frac{d\omega_{r1}}{dt} + B_1\omega_{r1} \quad (4)$$

where T_{e1} is the electromagnetic torque of the PM synchronous generator, J_1 is the moment of inertia of the PM synchronous generator and B_1 is the viscous friction coefficient of the PM synchronous generator.

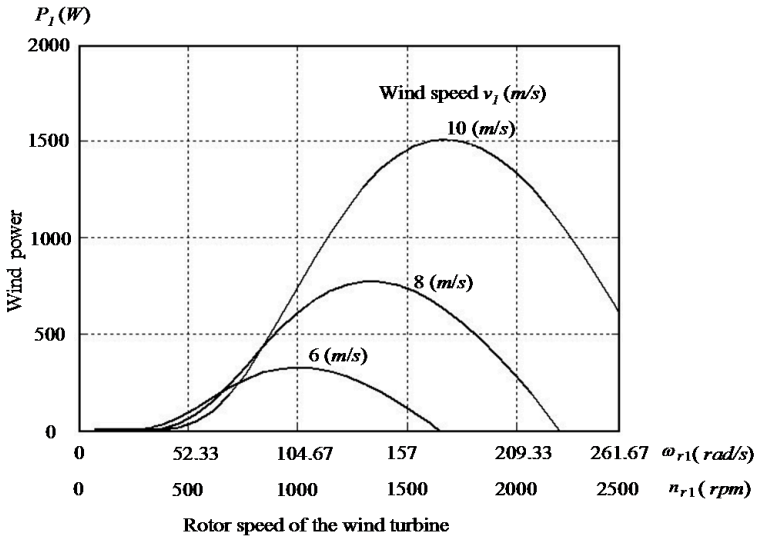

Figure 1. Characteristic curves of wind power *versus* rotor speed for WT model at different wind speeds.

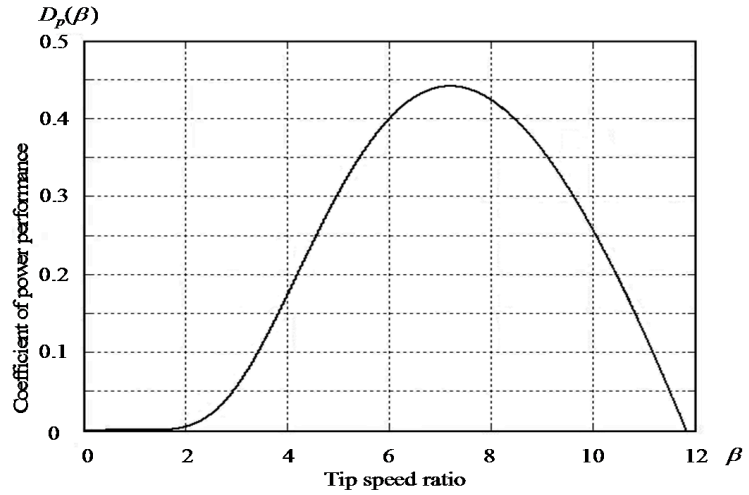

Figure 2. Characteristic curve of coefficient $D_p(\beta)$ of power performance *versus* tip ratio β for WT.

3.2. Model of PM Synchronous Generator

The voltage equations for the PM synchronous generator in the rotor reference frame can be indicated as follows [1,7–10]:

$$v_{q1} = -R_{s1}\, i_{q1} - L_{q1}\, \dot{i}_{q1} - P\omega_{r1} L_{d1} i_{d1}/2 + P\omega_{r1}\lambda_{pm}/2 \tag{5}$$

$$v_{d1} = -R_{s1}\, i_{d1} - L_{d1}\, \dot{i}_{d1} + P\omega_{r1} L_{q1}\, i_{q1}/2 \tag{6}$$

where v_{d1} is the d-axis stator voltage, v_{q1} is the q-axis stator voltage, i_{d1} is the d-axis stator current, i_{q1} is the q-axis stator current, L_{d1} is the d-axis stator inductance, L_{q1} is the q-axis stator inductance, R_{s1} is the stator resistance, and ω_{r1} is the rotor angular speed, respectively. The electromagnetic torque of the PM synchronous generator can be expressed as:

$$T_{e1} = \frac{3}{2}\frac{P}{2}\left[\lambda_{pm} i_{q1} - (L_{d1} - L_{q1}) i_{d1} i_{q1}\right] \tag{7}$$

where P is the number of poles, λ_{pm} is the permanent magnet flux linkage, $K_t = 3P\lambda_{pm}/4$ is the torque constant. In this paper, the control principle of the PM synchronous generator system is based on field-orirnted control [7–10]. The output power of the PM synchronous generator can be expressed as:

$$P_{out} = T_{e1}\omega_{r1} \tag{8}$$

where P_{out} is the output power of the PM synchronous generator.

3.3. Model of AC-DC Converter and DC-AC Converter

The system configuration of the WT driving a PM synchronous generator via AC-DC converter and DC-AC converter is shown in Figure 3. The block diagram of the control system is shown in Figure 3, where θ_{r1} is the rotor position of the PM synchronous generator, i_{dr}^* and i_{qr}^* are the d-axis and q-axis desired control currents of the rectifier, i_{ar}^*, i_{br}^* and i_{cr}^* are the desired phase currents of the PM synchronous generator in phases ar, br and cr, respectively, i_{ar}, i_{br} and i_{cr} are the measured phase currents of the PM synchronous generator in phases ar, br and cr, respectively, T_{ar}, T_{br} and T_{cr} are the sinusoidal pulse-width-modulation (SPWM) control signals of the rectifier in phases ar, br and cr, respectively, V_d is the measured magnitude of the DC bus voltage in output end of the rectifier, V_d^* is the desired magnitude of the DC bus voltage in output end of the rectifier, i_{di}^* and i_{qi}^* are the d-axis and q-axis desired control currents of the inverter, ω_{i1} is the electric angular frequency of the inverter at the load, θ_{i1} is the electric angular angle of the inverter at the load, i_{ai}^* , i_{bi}^* and i_{ci}^* are the desired phase currents of the inverter in phases ai, bi and ci, respectively, i_{ai}, i_{bi} and i_{ci} are the measured phase currents of the inverter in phases ai, bi and ci, respectively, v_{ai}, v_{bi} and v_{ci} are the measured phase voltages of the inverter in phases ai, bi and ci, respectively, T_{ai}, T_{bi} and T_{ci} are the sinusoidal pulse-width-modulation control signals of the inverter in phases ai; bi and ci, respectively, V_{rms} is the measured root-mean-square magnitude of the AC 60 Hz line voltage in output end of the inverter, V_{rms}^* is the desired root-mean-square magnitude of the AC 60 Hz line voltage in output end of the inverter; i_d is the measured DC bus current in output end of the rectifier, P_d is the measured DC bus power in output end of the rectifier, P_d^* is the desired DC bus power in output end of the rectifier, P_{out}^* is the maximum output power of the PM synchronous generator, η_{re} is the conversion efficiency of the rectifier which is 90%, η_{in} is the conversion efficiency of the inverter which is 90%, $P_d^* = \eta_{re} P_{out}^*$ is the command of the DC bus power in output end of the rectifier.

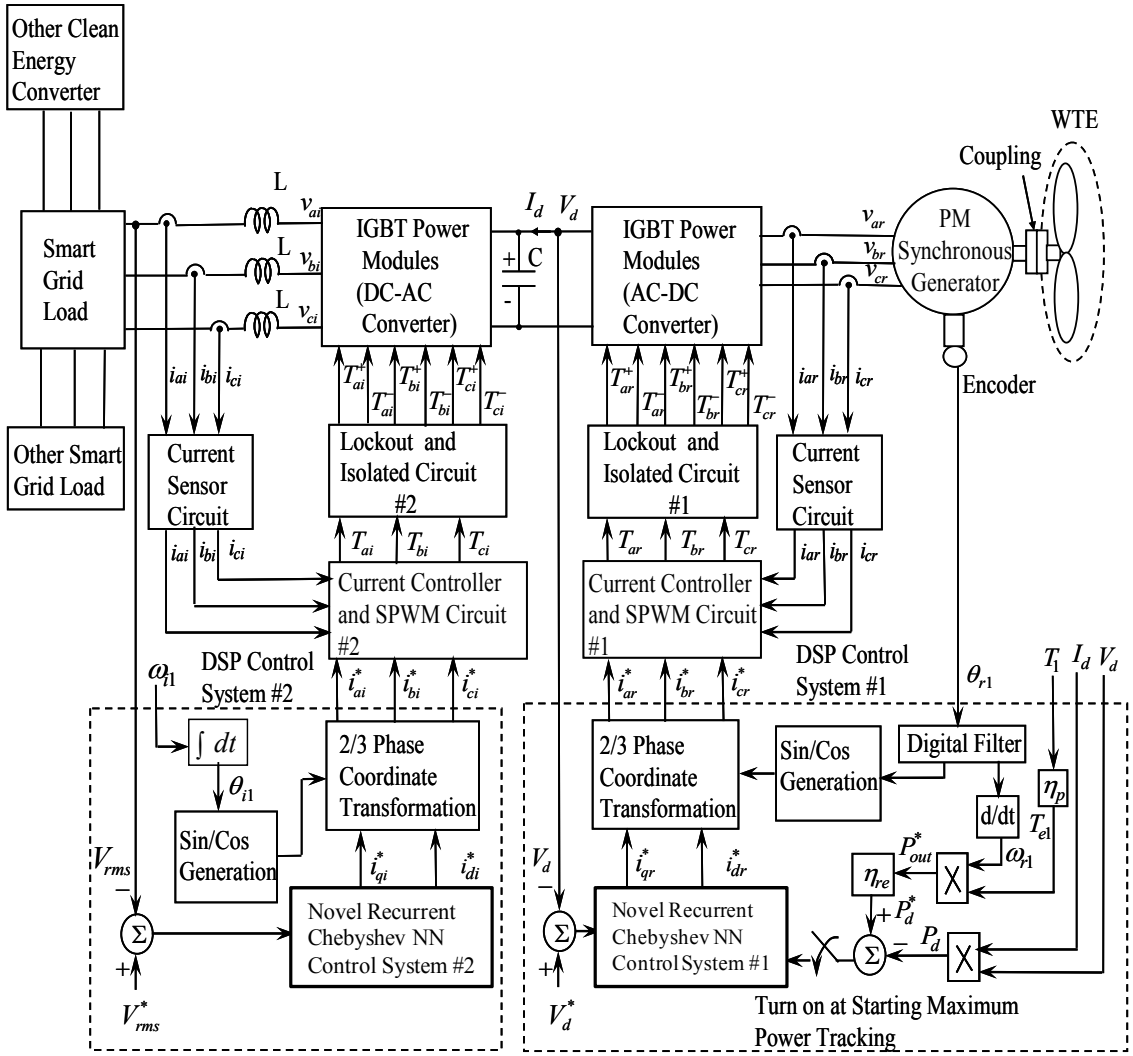

Figure 3. System configuration of the WT driving a PM synchronous generator system through AC-DC converter and a DC-AC converter using two sets of novel recurrent Chebyshev NN control systems.

The output voltage and output power of the AC-DC converter can be expressed as [10,35]:

$$V_d = \frac{3\sqrt{2}V_{abr}}{\pi}\cos\theta_\alpha = 1.35V_{abr}V_{cr}/V_P \tag{9}$$

$$P_d = V_d I_d = 1.35V_{abr}I_d\cos\theta_\alpha \tag{10}$$

where θ_α is the trigger angle in the power module of the AC-DC converter, V_{abr} is the output line voltage of the PM synchronous generator, V_{cr} is the control voltage of the AC-DC converter, and V_P is the peak value of the cosine wave of the AC-DC converter. Since this paper is dealing with an isolated system with maximum power control, the exceeding power must be consumed to yield system power balance. The more realistic way of control is to choose the DC voltage as the controlled variable. On the other hand, the DC-AC converter supplies the electrical power which is synchronized with the power system frequency. The output voltage and output power of the DC-AC converter can be expressed as [10,35].

$$V_{rms} = \frac{\sqrt{3}}{\sqrt{2}}m_a\frac{V_d}{2} = 0.612V_d m_a \tag{11}$$

$$P_{rms} = \sqrt{3}V_{rms}I_{rms} = 1.06V_d m_a I_{rms} \tag{12}$$

where m_a is the modulation ratio in the power module of the DC-AC converter, V_{rms} is the measured root-mean-square voltage in output end of the DC-AC converter; I_{rms} is the measured root-mean-square current in output end of the DC-AC converter, and P_{rms} is the root-mean-square power in output end of the DC-AC converter.

4. Design of the Novel Recurrent Chebyshev NN Control System

From Equations (9) and (11), the output voltage for the rectifier and the DC-AC converter provided by PM synchronous generator system can be expressed as [10,35]:

$$V_m = h_m \zeta_m, \ m = 1, 2 \tag{13}$$

where $V_1 = V_d$ is the output voltage of the rectifier, $V_2 = V_{rms}$ is the output voltage of the inverter, $h_1 = 1.35V_{abr}/V_P$ and $h_2 = 0.612V_d$ are the output voltage constants of the rectifier and the inverter, $\zeta_1 = V_{cr}$ and $\zeta_2 = m_a$ are regulating magnitudes of output voltage in the rectifier and the inverter. Since h_1 and h_2 are considered as constants, differentiating both sides of Equation (13) with respect to time yields.

$$\dot{V}_m = h_m \Delta\zeta_m = h_m u_m, \ m = 1, 2 \tag{14}$$

where $\Delta\zeta_m = u_m, \ m = 1, 2$ is the control effort of control system for the AC-DC converter and the AC-DC converter. The control problem of PM synchronous generator system is to control the change of control effort via the DC-AC converter and the DC-AC-DC converter so that the output voltage can provide a fixed voltage under the occurrence of the uncertainties such as the wide input voltages and load variations. The output error of voltage is defined as:

$$e_m = V_m^* - V_m, \ m = 1, 2 \tag{15}$$

where $V_1^* = V_d^*$ is the output reference voltage of the AC-DC converter and $V_2^* = V_{rms}^*$ is the output reference voltage of the DC-AC converter. The error $e_1 = V_1^* - V_1 = V_d^* - V_d$ is different between the reference DC voltage and the measured DC voltage of the AC-DC converter. The error $e_2 = V_2^* - V_2 = V_{rms}^* - V_{rms}$ is different between the reference AC voltage and the measured AC voltage of the DC-AC converter. If the system parameters are well known, the ideal controller can be designed as:

$$u_m^* = h_m^{-1}(\dot{V}_m^* + k_m e_m), \ m = 1, 2 \tag{16}$$

Combining Equations (14)–(16), then $\dot{e}_m + k_m e_m = h_m(u_m^* - u_m), \ m = 1, 2$. Taking Laplace transform, then $(s + k_m)e_m = F_m(s), \ m = 1, 2$, *i.e.*, $e_m = F_m/(s + k_m), \ m = 1, 2$. If $k_m, \ m = 1, 2$ is chosen to correspond to the coefficient of a Hurwitz polynomial $(s + k_m), \ m = 1, 2$, *i.e.*, a polynomial whose roots lie strictly in the open left half of the complex plane, then $\lim_{t\to\infty} e_m(t), \ m = 1, 2$. Since the system parameters may be unknown or perturbed, the ideal controller $u_m^*, \ m = 1, 2$ in Equation (16) can not be precisely implemented.

In order to efficiently control the output voltage of the PM synchronous generator system via the rectifier and the inverter, a block diagram of the novel recurrent Chebyshev NN control system with two sets of novel recurrent Chebyshev NNs as shown in Figure 4 is introduced in this paper.

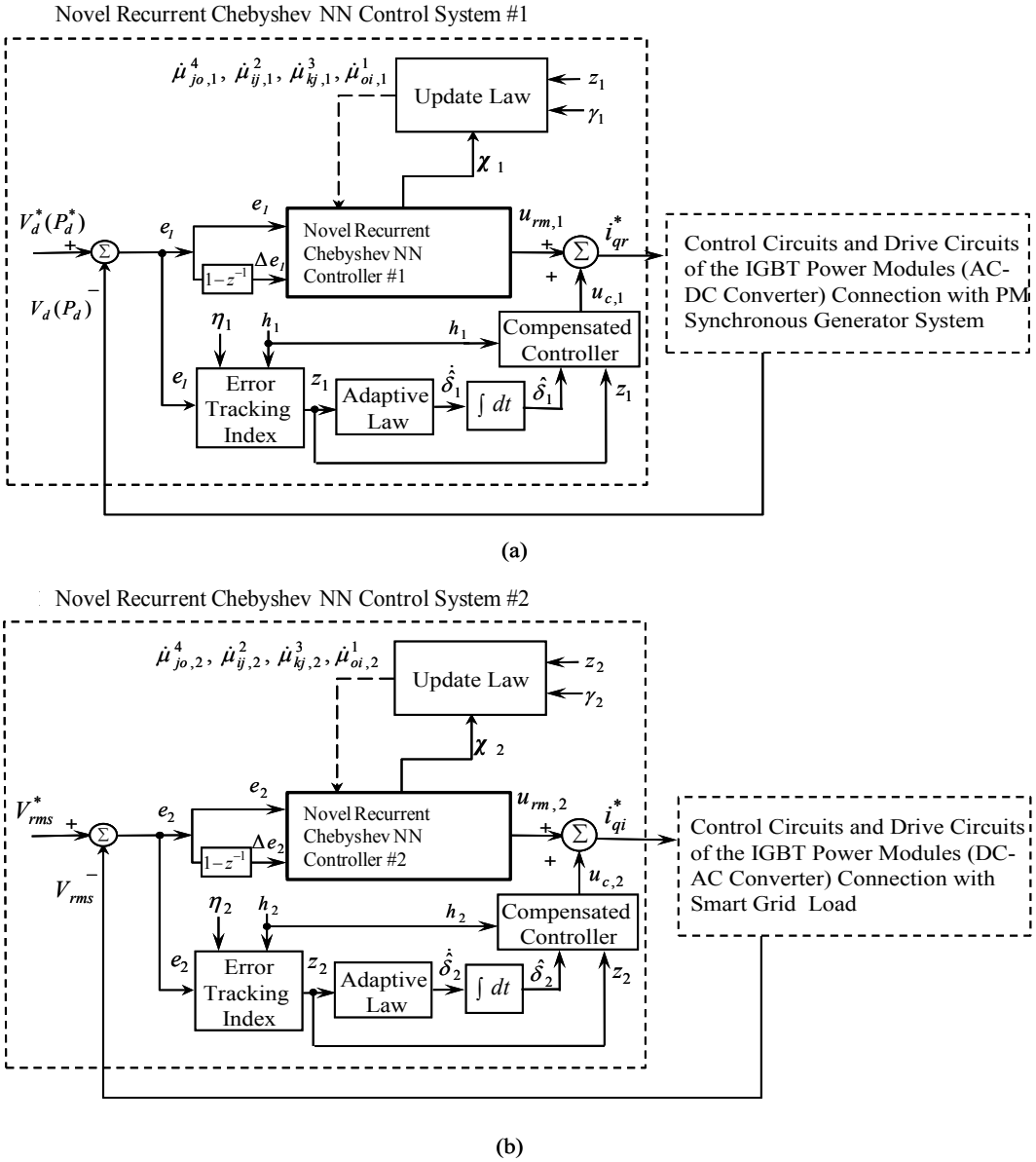

Figure 4. Block diagram of two sets of recurrent Chebyshev NN control systems for (**a**) AC-DC converter and (**b**) DC-AC converter.

The configuration of the recurrent Chebyshev NN control system consists of the recurrent Chebyshev NN controller and the compensated controller,

$$u_m = u_{rm,m} + u_{c,m},\ m = 1, 2 \tag{17}$$

where $u_{rm,m},\ m = 1, 2$ is the novel recurrent Chebshev NN controller for the AC-DC converter and the DC-AC converter and $u_{c,m},\ m = 1, 2$ is the compensated controller for the rectifier and the inverter. The recurrent Chebyshev NN controller is designed to mimic the ideal controller and the compensated controller is designed to compensate for the difference between the ideal controller and the novel recurrent Chebyshev NN controller. Substituting Equations (17) into (14), then

$$\dot{V}_m = h_m(u_{rm,m} + u_{c,m}),\ m = 1, 2 \tag{18}$$

the error equation governing the system can be obtained by combining Equations (15), (16) and (18), *i.e.*,

$$\dot{e}_m + k_m e_m = h_m(u_m^* - u_{rm,m} - u_{c,m}),\ m = 1, 2 \tag{19}$$

4.1. Description of Novel Recurrent Chebyshev NN

In the proposed four-layer novel recurrent Chebyshev NN with input layer using feedback signals from output layer are taken into account to result in better learning efficiency. The architecture of the four-layer novel recurrent Chebyshev NN shown in Figure 5 consists of the first layer (the input layer), the second layer (the Chebyshev layer), the third layer (the function layer) and the forth layer (the output layer). The exciting functions and signal propagations of nodes in each layer of the novel recurrent Chebyshev NN are explained as follows:

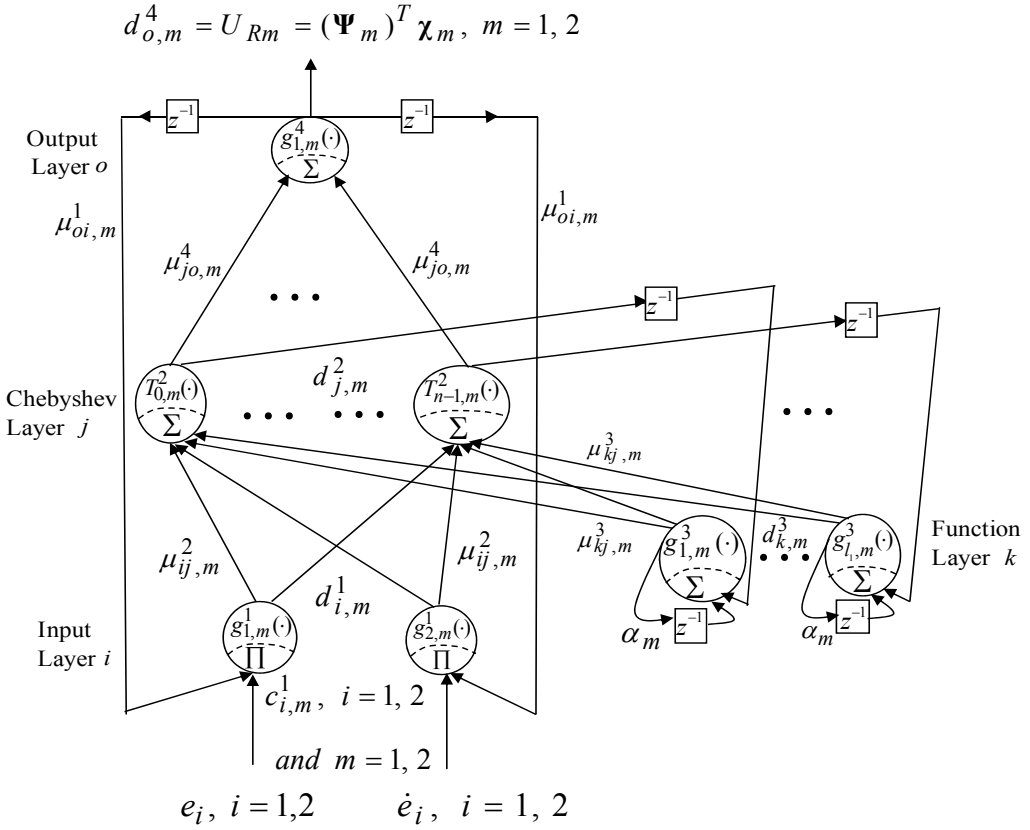

Figure 5. Architecture of the four-layer novel recurrent Chebyshev NN.

4.1.1. First Layer: Input Layer *i*

In the first layer, the input signals and the output signals for each node *i* in the *m*th novel recurrent Chebyshev NN can be expressed as:

$$\begin{aligned} node^1_{i,m}(N) &= \prod_o c^1_{i,m}(N) \cdot \mu^1_{oi,m} \cdot d^4_{o,m}(N-1), \\ d^1_{i,m}(N) &= g^1_{i,m}(node^1_{i,m}(N)), i = 1, 2\ and\ m = 1, 2 \end{aligned} \tag{20}$$

where $c^1_{i,m}$ is the input of the *i*th node in the *m*th novel recurrent Chebyshev NN, $d^1_{i,m}$ is the output of the *i*th node in the *m*th novel recurrent Chebyshev NN, $\mu^1_{oi,m}$ is the recurrent weight between output layer and input layer in the *m*th novel recurrent Chebyshev NN, and $d^4_{o,m}$ is the output value of the output layer in the *m*th recurrent Chebyshev NN. The different inputs of the two sets of novel recurrent Chebyshev NNs are $c^1_{1,1} = e_1 = V_d^* - V_d$, $c^1_{2,1} = \dot{e}_1 \cong (1 - z^{-1})\Delta e_1$ for the rectifier, and

$c^1_{1,2} = e_2 = V^*_{rms} - V_{rms}$, $c^1_{2,2} = \dot{e}_2 \cong (1 - z^{-1})\Delta e_2$ for the DC-AC converter, respectively. The N indicates the number of iterations.

4.1.2. Second Layer: Chebyshev Layer j

In the second layer, the input signals and the output signals for each node jth in the mth novel recurrent Chebyshev NN can be expressed as:

$$\begin{gathered} node^2_{j,m}(N) = \sum_k \mu^3_{kj,m} \cdot d^3_{k,m}(N) + \sum_i \mu^2_{ij,m} \cdot d^1_{i,m}(N), \\ d^2_{j,m}(N) = g^2_{j,m}\left(node^2_{j,m}(N)\right) = T^2_{j,m}(node^2_{j,m}(N)) \qquad j = 0, 1, \ ..., n-1 \ and \ m = 1, 2 \end{gathered} \tag{21}$$

where $T_j(\cdot)$ is the Chebyshev polynomial [25,26] which is selected as activation function of the Chebyshev layer; $\mu^3_{kj,m}$ is the connective weight between hidden layer and Chebyshev layer in the mth novel recurrent Chebyshev NN, $\mu^2_{ij,m}$ is the connective weight between the input layer and the Chebyshev layer in the mth novel recurrent Chebyshev NN, n is the number of neurons in the Chebyshev layer, $g^2_{j,m}$ is the activation function, which is the Chebyshev polynomial function in the mth novel recurrent Chebyshev NN, $d^1_{i,m}(N)$ is the ith output node of input layer in the mth novel recurrent Chebyshev NN, $d^3_{k,m}(N)$ is the kth output to the node of hidden layer in the mth novel recurrent Chebyshev NN, and $d^2_{j,m}$ is the jth output nod of Chebshev layer in the mth novel recurrent Chebyshev NN. The first few Chebyshev polynomials are given by $T_0(x) = 1$, $T_1(x) = x$ and $T_2(x) = 2x^2 - 1$. The higher order Chebyshev polynomials may be generated by the recursive formula given by $T_{n+1}(x) = 2xT_n(x) - T_{n-1}(x)$.

4.1.3. Third Layer: Function Layer k

In the third layer, the input signals and the output signals for each node kth in the mth novel recurrent Chebyshev NN can be expressed as:

$$\begin{gathered} node^3_{k,m}(N) = d^2_{j,m}(N-1) + \alpha_m \, d^3_{k,m}(N-1), \\ d^3_{k,m}(N) = g^3_{k,m}(node^3_{k,m}(N)), \ k = 1, \cdots, \ l_1 \ and \ m = 1, \ 2 \end{gathered} \tag{22}$$

where $d^2_{j,m}(N)$ is the jth output node of Chebyshev layer in the mth novel recurrent Chebyshev NN, $g^3_{k,m}$ is the activation function, which is the linear function in the mth novel recurrent Chebyshev NN, $d^3_{k,m}(N)$ is the kth output to the node of hidden layer in the mth novel recurrent Chebyshev NN, l_1 is the number of neurons in the hidden layer, and $0 \leqslant \alpha_m < 1$ is the self-connecting feedback gain of function layer.

4.1.4. Fourth Layer: output Layer o

In the fourth layer, the input signals and the output signals for node oth in the mth novel recurrent Chebyshev NN are expressed as:

$$\begin{gathered} node^4_{o,m}(N) = \sum_j \mu^4_{jo,m} \cdot d^2_{j,m}(N), \\ d^4_{o,m}(N) = g^4_{o,m}(node^4_{o,m}(N)), o = 1 \ and \ m = 1, 2 \end{gathered} \tag{23}$$

where $\mu^4_{jo,m}$ is the connective weights between the function layer and the output layer in the mth novel recurrent Chebyshev NN (*i.e.*, the output action intensity of the oth output associated with the jth node in the mth novel recurrent Chebyshev NN), and $d^2_{j,m} = c^4_{j,m}$ is the jth output node of Chebyshev layer in the mth novel recurrent Chebyshev NN. The single node oth in this layer is indicated as summation$\sum$. The output in the mth novel recurrent Chebyshev NN can be can be expressed as:

$$d^4_{o,m} = (\mathbf{\Psi}_m)^T \boldsymbol{\chi}_m, m = 1, 2 \tag{24}$$

The output values of the two sets of four-layer novel recurrent Chebyshev NNs can be rewritten as $U_{R\,1} = (\mathbf{\Psi}_1)^T \chi_1 = i_{qr}^*$ for the AC-DC converter and $U_{R\,2} = (\mathbf{\Psi}_2)^T \chi_2 = i_{qi}^*$ for the DC-AC converter. Two sets of vectors $\mathbf{\Psi}_1 = \begin{bmatrix} \mu_{11,1}^4 & \mu_{21,1}^4 & \cdots & \mu_{n1,1}^4 \end{bmatrix}^T$ and $\mathbf{\Psi}_2 = \begin{bmatrix} \mu_{11,2}^4 & \mu_{21,2}^4 & \cdots & \mu_{n1,2}^4 \end{bmatrix}^T$ are the adjustable parameters between the function layer and the output layer in the two sets of four-layer novel recurrent Chebyshev NNs. Two sets of vectors $\chi_1 = \begin{bmatrix} c_{1,1}^4 & c_{2,1}^4 & \cdots & c_{n,1}^4 \end{bmatrix}^T$ and $\chi_2 = \begin{bmatrix} c_{1,2}^4 & c_{2,2}^4 & \cdots & c_{n,2}^4 \end{bmatrix}^T$ are the inputs vectors of the output layer in the two sets of four-layer novel recurrent Chebyshev NNs, in which $c_{j,m}^4$ is determined by the selected Chebyshev polynominal function and $0 \leqslant c_{j,m}^4 \leqslant 1$.

4.2. Controller Design

The novel recurrent Chebyshev NN controller is designed to estimate the ideal controller in Equation (16). By the universal approximation theorem [36], there exists the ideal neural controller $u_{rm,m}^*,\ m = 1, 2$ such that

$$u_m^* = u_{rm,m}^* + \varepsilon_m = (\mathbf{\Psi}_m^*)^T \chi_m + \varepsilon_m,,\ m = 1, 2 \tag{25}$$

where $\varepsilon_m,\ m = 1, 2$ is a minimum approximation error and $\mathbf{\Psi}_m^*, m = 1, 2$ is the ideal parameter vector of $\mathbf{\Psi}_m, m = 1, 2$. The approximation error $\varepsilon_m, m = 1, 2$ is assumed to be bounded by a positive constant $\delta_m, m = 1, 2$ (*i.e.*, $|\varepsilon_m| \leqslant \delta_m, m = 1, 2$). This approximation error bound $\delta_m,\ m = 1, 2$ is generally unobtainable in practical applications, so that it will be estimated in the following derivations. Moreover, the ideal recurrent Chebyshev NN controller cannot be obtained, so that an on-line estimation novel recurrent Chebyshev NN controller is defined as:

$$u_{rm,m} = \left(\widehat{\mathbf{\Psi}}_m\right)^T \chi_m, \quad m = 1, 2 \tag{26}$$

where $\widehat{\mathbf{\Psi}}_m,\ m = 1, 2$ is an estimate of the ideal parameter vector $\mathbf{\Psi}_m^*,\ m = 1, 2$. Define the estimation error $\widetilde{\mathbf{\Psi}}_m,\ m = 1, 2$ as:

$$\begin{aligned} \widetilde{u}_{rm,m} &= u_m^* - u_{rm,m} = u_{rm,m}^* + \varepsilon_m - u_{rm,m} \\ &= (\mathbf{\Psi}_m^*)^T \chi_m + \varepsilon_m - \left(\widehat{\mathbf{\Psi}}_m\right)^T \chi_m = [\mathbf{\Psi}_m^* - \widehat{\mathbf{\Psi}}_m]^T \chi_m + \varepsilon_m \\ &= \left(\widetilde{\mathbf{\Psi}}_m^*\right)^T \chi_m + \varepsilon_m, \quad m = 1, 2 \end{aligned} \tag{27}$$

where $\widetilde{\mathbf{\Psi}}_m^* = \mathbf{\Psi}_m^* - \widehat{\mathbf{\Psi}}_m,\ m = 1, 2$. Define the error tracking index as:

$$z_m = e_m + k_m \int_0^t e_m d\tau, \quad m = 1, 2 \tag{28}$$

Differentiating both sides of Equation (23) with respect to time yields

$$\dot{z}_m = \dot{e}_m + k_m e_m, \quad m = 1, 2 \tag{29}$$

Then, the error (19) can be rewritten as:

$$\begin{aligned} \dot{z}_m &= h_m(u_m^* - u_{rm,m} - u_{c,m}) \\ &= h_m[\left(\widetilde{\mathbf{\Psi}}_m^*\right)^T \chi_m + \varepsilon_m - u_{c,m}],\ m = 1, 2 \end{aligned} \tag{30}$$

To relax the requirement of the uncertain bound $\delta_m, m = 1, 2$, the bound estimation mechanism is developed to observe the bound of the approximation error. Define the estimation error of the bound:

$$\widetilde{\delta}_m = \delta_m - \widehat{\delta}_m, m = 1, 2 \tag{31}$$

where $\widehat{\delta}_m, m = 1, 2$ is the estimation of uncertain bound. To guarantee the stability of the adaptive novel recurrent Chebyshev NN control scheme, the Lyapunov function candidate is defined as:

$$L_{1,m}(z_m, \widetilde{\mathbf{\Psi}}_m, \widetilde{\delta}_m) = z_m^2/2 + \widetilde{\delta}_m^2/(2\eta_m) + h_m \widetilde{\mathbf{\Psi}}^T \widetilde{\mathbf{\Psi}}/(2\gamma_m),\ m = 1, 2 \tag{32}$$

where $\eta_m,\ m = 1, 2$ is a constant learning rate, and $\gamma_m,\ m = 1, 2$ is a variable learning rate, which will be discussed in the following subsection to speed up the convergence of novel recurrent Chebyshev NN controller parameter. Differentiating Equation (32) with respect to time and using Equation (30), we get:

$$\begin{aligned} \dot{L}_{1,m}(z_m, \widetilde{\mathbf{\Psi}}_m, \widetilde{\delta}_m) &= z_m \dot{z}_m + h_m \widetilde{\delta}_m \dot{\widetilde{\delta}}_m/\eta_m + h_m \widetilde{\mathbf{\Psi}}^T \dot{\mathbf{\Psi}}/\gamma_m \\ &= z_m \{h_m [\left(\widetilde{\mathbf{\Psi}}_m^*\right)^T \boldsymbol{\chi}_m + \varepsilon_m - u_{c,m}]\} + h_m \widetilde{\delta}_m \dot{\widetilde{\delta}}_m/\eta_m + h_m \left(\widetilde{\mathbf{\Psi}}_m^*\right)^T \dot{\mathbf{\Psi}}_m/\gamma_m \\ &= h_m \left(\widetilde{\mathbf{\Psi}}_m^*\right)^T \left(z_m \boldsymbol{\chi}_m + \dot{\mathbf{\Psi}}_m/\gamma_m\right) + z_m h_m \left(\varepsilon_m - u_{c,m}\right) + h_m \widetilde{\delta}_m \dot{\widetilde{\delta}}_m/\eta_m \\ &= \{h_m \left(\widetilde{\mathbf{\Psi}}_m^*\right)^T \left(z_m \boldsymbol{\chi}_m + \dot{\mathbf{\Psi}}_m/\gamma_m\right)\} + z_m h_m \left(\varepsilon_m - u_{c,m}\right) + h_m \widetilde{\delta}_m \dot{\widetilde{\delta}}_m/\eta_m,\ m = 1, 2 \end{aligned} \tag{33}$$

For achieving $\dot{L}_{1,m} \leqslant 0,\ m = 1, 2$, the adaptive laws and the compensated controller are chosen as:

$$u_{c,m} = \widehat{\delta}_m \mathrm{sgn}\left(z_m h_m\right),\ m = 1, 2 \tag{34}$$

$$\dot{\widetilde{\Psi}}_m = -\dot{\widehat{\Psi}}_m = -\gamma_m \left(z_m \boldsymbol{\chi}_m\right),\ m = 1, 2 \tag{35}$$

$$\dot{\widetilde{\delta}}_m = -\dot{\widehat{\delta}}_m = -\eta_m \left|z_m\right| \mathrm{sgn}\left(h_m\right),\ m = 1, 2 \tag{36}$$

where $\mathrm{sgn}(\cdot)$ is the sign function. Substituting Equations (34)–(36) into (33), then Equation (33) can be rewritten as:

$$\begin{aligned} \dot{L}_{1,m}(z_m, \widetilde{\mathbf{\Psi}}_m, \widetilde{\delta}_m) &= z_m h_m \varepsilon_m - \widehat{\delta}_m \left|z_m h_m\right| - (\delta_m - \widehat{\delta}_m) \left|z_m h_m\right| \\ &= z_m h_m \varepsilon_m - \delta_m \left|z_m h_m\right| \\ &\leqslant -(\delta_m - \varepsilon_m) \left|z_m h_m\right| \leqslant 0,\ m = 1, 2 \end{aligned} \tag{37}$$

Since $\dot{L}_{1.m}(z_m, \widetilde{\mathbf{\Psi}}_m, \widetilde{\delta}_m) \leqslant 0,\ m = 1, 2$ is the negative semidefinite, that is $L_{1,m}(z_m(t), \widetilde{\mathbf{\Psi}}_m(t), \widetilde{\delta}_m(t)) \leqslant L_{1,m}(z_m(0), \widetilde{\mathbf{\Psi}}_m(0), \widetilde{\delta}_m(0)),\ m = 1, 2$, it implies that $z_m(t)$, $\widetilde{\mathbf{\Psi}}_m(t)$ and $\widetilde{\delta}_m(t)$ are bounded. Let function $\varphi_m(t) = (\delta_m - \varepsilon_m) \left|z_m h_m\right| \leqslant -\dot{L}_{1,m},\ m = 1, 2$, and integrate $\varphi_m(t)$ with respect to time, then it is obtained that:

$$\int_0^t \varphi_m(\tau) d\tau \leqslant L_{1,m}(z_m(0), \widetilde{\mathbf{\Psi}}_m(0), \widetilde{\delta}_m(0)) - L_{1,m}(z_m(t), \widetilde{\mathbf{\Psi}}_m(t), \widetilde{\delta}_m(t)),\ m = 1, 2 \tag{38}$$

Because $L_{1,m}(z_m(0), \widetilde{\mathbf{\Psi}}_m(0), \widetilde{\delta}_m(0)),\ m = 1, 2$ is bounded, and $L_{1,m}(z_m(t), \widetilde{\mathbf{\Psi}}_m(t), \widetilde{\delta}_m(t)),\ m = 1, 2$ is nonincreasing and bounded, the following result can be obtained:

$$\lim_{t \to \infty} \int_0^t \varphi_m(\tau) d\tau \leqslant \infty,\ m = 1, 2 \tag{39}$$

Moreover, since $\dot{\varphi}_m(t),\ m = 1, 2$ is bounded, by Barbalat's Lemma [37] $\lim_{t\to\infty} \varphi_m(t) = 0,\ m = 1, 2$. That is, $z_m \to 0,\ m = 1, 2$ as $t \to 0$. As a result, the stability of the proposed recurrent Chebyshev NN control system can be guaranteed.

4.3. Convergence Analyses

The adaptive law shown in Equation (35) calls for a proper choice of the learning rate. In order to train the novel recurrent Chebyshev NN efficiently, an ideal learning rate will be derived to achieve the fast convergence of output tracking error. First, the adaptive law shown in Equation (35) can be rewritten as:

$$\dot{\hat{\mu}}^4_{jo,m}(N) = \gamma_m \cdot z_m \cdot c^4_{j,m},\ m = 1, 2 \tag{40}$$

The central part of the training algorithm for the novel recurrent Chebyshev NN concerns how to obtain recursively a gradient vector in which each element in the training algorithm is defined as the derivative of an energy function with respect to a parameter of the network. In order to describe the online training algorithm of the novel recurrent Chebyshev NN, a cost function is defined as:

$$V_{c,m} = \frac{1}{2} e^2_m, m = 1, 2 \tag{41}$$

According to the gradient descent method, the adaptive law of the weight also can be represented as:

$$\begin{aligned} \dot{\hat{\mu}}^4_{jo,m}(N) &= -\gamma_m \frac{\partial V_{c,m}}{\partial \hat{\mu}^4_{jo,m}(N)} \\ &= -\gamma_m \frac{\partial V_{c,m}}{\partial d^4_{o,m}} \frac{\partial d^4_{o,m}}{\partial node^4_{o,m}(N)} \frac{\partial node^4_{o,m}(N)}{\partial, \hat{\mu}^4_{jo,m}(N)} \\ &= -\gamma_m \frac{\partial V_{c,m}}{\partial d^4_{o,m}} c^4_{j,m},\ m = 1, 2 \end{aligned} \tag{42}$$

Comparing Equation (40) with (42), yields $\partial V_{c,m}/\partial d^4_{o,m} = -z_m,\ m = 1, 2$. The propagated error term can be calculation as:

$$\rho_{j,m} \triangleq -\frac{\partial V_{c,m}}{\partial d^4_{o,m}} \frac{\partial d^4_{o,m}}{\partial node^4_{o,m}} \frac{\partial node^4_{o,m}}{\partial d^2_{j,m}} = z_m \mu^4_{jo,m},\ m = 1, 2 \tag{43}$$

The connective weight $\mu^3_{kj,m},\ m = 1, 2$ between context layer and hidden layer can be updated as:

$$\begin{aligned} \dot{u}^3_{kj,m} &= -\frac{\partial V_{c,m}}{\partial u^3_{kj,m}} = -\frac{\partial V_{c,m}}{\partial d^4_{o,m}} \frac{\partial d^4_{o,m}}{\partial node^4_{o,m}} \frac{\partial node^4_{o,m}}{\partial d^2_{j,m}} \frac{\partial d^2_{j,m}}{\partial node^2_{j,m}} \frac{\partial node^2_{j,m}}{\partial u^3_{kj,m}} \\ &= \rho_{j,m} P_{j,m},\ m = 1, 2 \end{aligned} \tag{44}$$

where $P_{j,m} \equiv \partial d^2_{j,m}/\partial u^3_{kj,m}$ can be calculate from Equation (21).

The connective weight $\mu^2_{ij,m},\ m = 1, 2$ between hidden layer and input layer can be updated as:

$$\begin{aligned} \dot{u}^2_{ij,m} &= -\frac{\partial V_{c,m}}{\partial u^2_{ij,m}} = -\frac{\partial V_{c,m}}{\partial d^4_{o,m}} \frac{\partial d^4_{o,m}}{\partial node^4_{o,m}} \frac{\partial node^4_{o,m}}{\partial d^2_{j,m}} \frac{\partial d^2_{j,m}}{\partial node^2_{j,m}} \frac{\partial node^2_{j,m}}{\partial u^2_{ij,m}} \\ &= \rho_{j,m} Q_{j,m},\ m = 1, 2 \end{aligned} \tag{45}$$

where $Q_{j,m} \equiv \partial d^2_{j,m}/\partial u^2_{ij,m},\ m = 1, 2$ can be calculate from Equation (21).

The recurrent weight $\mu^1_{oi,m},\ m = 1, 2$ between output layer and input layer can be updated as:

$$\begin{aligned} \dot{u}^1_{oi,m} &= -\frac{\partial V_{c,m}}{\partial u^1_{oi,m}} = -\frac{\partial V_{c,m}}{\partial d^4_{o,m}} \frac{\partial d^4_{o,m}}{\partial node^4_{o,m}} \frac{\partial node^4_{o,m}}{\partial d^2_{j,m}} \frac{\partial d^2_{j,m}}{\partial node^2_{j,m}} \frac{\partial node^2_{j,m}}{\partial u^1_{oi,m}} \\ &= \rho_{j,m} R_{j,m},\ m = 1, 2 \end{aligned} \tag{46}$$

where $R_{j,m} \equiv \partial d^2_{j,m}/u^1_{oi,m}$, $m = 1, 2$ can be calculate from Equation (20). Then, the convergence analysis in the following theorem is to derive specific learning rate to assure convergence of the output tracking error.

Theorem 1. *Let γ_m, $m = 1, 2$ be the learning rate of the recurrent Chebyshev NN weight, and let $P_{w\,max,m}$, $m = 1, 2$ be defined as $P_{w\,max,m} \equiv max_N \| P_{w,m}(N) \|$, $m = 1, 2$, where $P_{w,m}(N) = \partial d^4_{o,m}/\partial \mu^4_{ko,m}$, $m = 1, 2$ and $\| \cdot \|$ is the Euclidean norm in $\Re^n$. Then, the convergence of the output tracking error is guaranteed if the learning rate γ_m, $m = 1, 2$ is chosen as:*

$$0 < \gamma_m < \frac{2}{(P_{w\max,m})^2 [z_m/e_m(N)]^2}, \; m = 1, 2 \tag{47}$$

Moreover, the ideal learning rate which achieves the fast convergence can be obtained as:

$$\gamma^*_m = \frac{1}{(P_{w\max,m})^2 [z_m/e_m(N)]^2}, \; m = 1, 2 \tag{48}$$

Proof. Since

$$P_{w,m}(N) = \frac{\partial d^4_{o,m}}{\partial \mu^4_{ko,m}} = c^4_{j,m}, \; m = 1, \; 2 \tag{49}$$

then, a discrete-type Lyapunov function is selected as:

$$L_{2,\,m}(N) = \frac{1}{2} e^2_m(N), \; m = 1, 2 \tag{50}$$

the change in the Lyapunov function is obtained by:

$$\Delta L_{2,m}(N) = L_{2,m}(N+1) - L_{2,m}(N) = \frac{1}{2}\left[e^2_m(N+1) - e^2_m(N)\right], \; m = 1, 2 \tag{51}$$

the error difference can be represented by [18].

$$e_m(N+1) = e_m(N) + \Delta e_m(N) = e_m(N) + \left[\frac{\partial e_m(N)}{\partial \mu^4_{ko,m}}\right]^T \Delta \mu^4_{ko,m}, \; m = 1, 2 \tag{52}$$

where $\Delta e_m(N)$ is the output error change and $\Delta \mu^4_{ko,m}$ represents change of the weight. Using Equations (40)–(42) and (49), then Equation (52) can be obtained:

$$\frac{\partial e_m(N)}{\partial \mu^4_{ko,m}} = \frac{\partial e_m(N)}{\partial V_{c,m}} \frac{\partial V_{c,m}}{\partial d^4_{o,m}} \frac{\partial d^4_{o,m}}{\partial \mu^4_{ko,m}} = -\frac{z_m}{e_m(N)} P_{w,m}(N), \; m = 1, \; 2 \tag{53}$$

$$e_m(N+1) = e_m(N) - \left[\frac{z_m}{e_m(N)} P_{w,m}(N)\right]^T \gamma_m z_m P_{w,m}(N), \; m = 1, \; 2 \tag{54}$$

Thus

$$\begin{aligned} \| e_m(N+1) \| &= \left\| e_m(N)\left[1 - \gamma_m (z_m/e_m(N))^2 P^T_{w,m}(N) P_{w,m}(N)\right] \right\| \\ &\leqslant \| e(N) \| \left\| 1 - \gamma_m (z_m/e_m(N))^2 P^T_{w,m}(N) P_{w,m}(N) \right\|, \; m = 1, \; 2 \end{aligned} \tag{55}$$

from Equation (51) to (55), $\Delta L_{2,m}(N)$, $m = 1, 2$ can be rewritten as:

$$\begin{aligned} \Delta L_{2,m}(N) &= \tfrac{1}{2}\gamma_m [z_m/e_m(N)]^2 P^T_{w,m}(N) P_{w,m}(N) \left\{\gamma_m [z_m/e_m(N)]^2 P^T_{w,m}(N) P_{w,m}(N) - 2\right\} \\ &\leqslant \tfrac{1}{2}\gamma_m [z_m/e_m(N)]^2 \left(P_{w\max,m}(N)\right)^2 \left\{\gamma_m [z_m/e_m(N)]^2 \left(P_{w\max,m}(N)\right)^2 - 2\right\}, \; m = 1, \; 2 \end{aligned} \tag{56}$$

If γ_m, $m = 1, 2$ is chosen as $0 < \gamma_m < 2/\{(P_{w\max,m})^2[z_m/e_m(N)]^2\}$, $m = 1, 2$, then the Lyapunov stability of $L_{2,m}(N) > 0$, $m = 1, 2$ and $\Delta L_{2,m}(N) < 0$, $m = 1, 2$ is guaranteed so that the output tracking error will converge to zero as $t \to 0$. This completes the proof of the theorem. Moreover, the ideal learning rate which achieves the fast convergence is corresponding to $2\gamma_m^*\{(P_{w\max,m})^2[z_m/e_m(N)]^2\} - 2 = 0$, $m = 1, 2$, *i.e.*,

$$\gamma_m^* = 1/\{(P_{w\max,m})^2[z_m/e_m(N)]^2\},\ m = 1, 2 \tag{57}$$

which comes from the derivative of Equation (56) with respect to γ_m, $m = 1, 2$ and equals to zero. This shows an interesting result for the ideal learning rate which can be online tuned at each instant. In summary, the on-line learning algorithm of the novel recurrent Chebyshev NN controller is based on the adaptive law Equation (35) for the weight adjustment with the ideal learning rate in Equation (48).

5. Experimental Results

The configure of the PM synchronous generator system shown in Figure 3 consists of two sets of field-oriented institutions, two sets of current control loops, two sets of SPWM control circuits, two sets of interlock and isolated circuits, two sets of isolated-gate bipolar transistor (IGBT) power modules (*i.e.*, the AC-DC converter and the DC-AC converter), and two sets of recurrent Chebyshev NN control systems. The output DC voltage of the AC-DC converter, which is provided by WT driving PM synchronous generator system, is controlled by the novel recurrent Chebyshev NN control system # 1. Then, the output AC 60 Hz line voltage of the DC-AC conveter controlled by the novel recurrent Chebyshev NN control system #2 is provided to smart grid power system. The specification of PM synchronous generator is a three-phase four-pole 1.5 kW 220 V 10 A 2000 rpm type for experimental test in this paper. The electric parameters of the drive model at the nominal condition are $R_{s1} = 0.2\Omega$, $L_{d1} = L_{q1} = 6mH$, $\lambda_{pm} = 0.46\,Wb - T$. Both output voltages of the AC-DC converter and the DC-AC converter, which are controlled by two sets of novel recurrent Chebyshev NN control systems, are implemented by using two sets of TMS320C32 DSP (Spinel Tech. Co., Taipei, Taiwan) control boards and interface cards.

The voltage and power control of the PM synchronous generator system, which controlled by using two sets of novel recurrent Chebyshev NN control systems, are realized by two sets of TMS320C32 DSP control systems. For implementing two sets of current-controlled PWM AC-DC converter and DC-AC converter, two sets of IGBT power modules are adopted six pices of GBSM 100GB-120DLC manufactured by Eupec Co. (Warstein, Germany). The switching frequency of IGBT power modules is 15 kHz. The recurrent Chebyshev NN has 2, 3, 3, 1 nodes in the input layer, the Chebyshev layer, the function layer and the output layer, respectively. The parameters in the novel recurrent Chebyshev NN control system are chosen to achieve the best transient control performance in experimentation considering the requirement of stability. Usually, some heuristics can be used to roughly initialize the parameters of the novel recurrent Chebyshev NN for practical application. The effect due to the inaccurate selection of the initialized parameters can be retrieved by the online parameter training methodology. For simplicity, the all recurrent weights between the output layer and the input layer in the two sets of novel recurrent Chebyshev NNs are to set 1. Moreover, the connective weights between the hidden layer and the Chebyshev layer, the connective weights between the input layer and the Chebyshev layer, and the connective weights between the Chebyshev layer and the output layer in the two sets of novel recurrent Chebyshev NNs are initialized with random numbers. Furthermore, the normalized inputs and references have zero and unity, respectively. In addition, the network outputs should be converted back to the original units of the references. The parameters adjustment process remains continually active for the duration of the experimentation. To satisfy specification of the grid load and regulate of output voltage in the DC-AC converter controlled by the novel recurrent Chebyshev NN control system, the reference V_d^* of DC bus voltage is selected as twice of the reference V_{rms}^* of output AC line voltage in the output end of the inverter. Since the maximum

voltage of the output AC line voltage is $110\sqrt{2}$ = 155 V. Consider the line voltage drop and switching devices (IGBT) of the inverter, the reference for V_d^* is selected as 220 V. Therefore, the output voltage V_{rms} of the inverter controlled by the novel recurrent Chebyshev NN control system can be regulated as 110 V root-mean-square (RMS) voltage to satisfy specification of the three-phase load. Firstly, the rotor speed ω_{r1} (n_{r1}), the step desired DC bus voltage V_d^*, the step desired root-mean-square AC 60 Hz line voltage V_{rms}^* under light load are set as 78.5 rad/s (750 rpm), 220 V and 110 V, respectively, Secondly, the rotor speed ω_{r1} (n_{r1}), the step desired DC bus voltage V_d^*, the step desired root-mean-square AC 60 Hz line voltage V_{rms}^* under heavy load are set as 157 rad/s (n_{r1} = 1500 rpm), 220 V and 110 V, respectively. Both light load and heavy load patch powers as 121W and 242W, respectively. Some experimental results of the WT driving PM synchronous generator system using the two sets of PI controllers are demonstrated for the comparison of the control performance. Since the PM synchronous generator system is a nonlinear and time-varying system, the gains of the two sets of PI controllers for both the DC bus voltage adjustment and AC 60 Hz line voltage adjustment are obtained by trial and error to achieve steady state control performance. The control gains of the two sets of PI controllers are $K_p = 5.2,\ K_i = 10.2$ for the DC bus voltage adjustment and $K_p = 4.8,\ K_i = 10.8$ for the AC 60 Hz line voltage adjustment.

The experimental results of the WT driving PM synchronous generator system using two sets of PI controllers under light load (*i.e.*, Δ connection three-phase load of 100 Ω) for ω_{r1} = 78.5 rad/s (n_{r1} = 750 rpm) are shown in Figure 6. The responses of the rotor speed ω_{r1} (n_{r1}), the step desired DC bus voltage V_d^* and the measured DC bus voltage V_d in output end of the rectifier, the step desired root-mean-square AC 60 Hz line voltage V_{rms}^* and the measured root-mean-square AC 60 Hz line voltage V_{rms} in output end of the inverter, the steady-state desired phase current i_{ai}^* and the measured phase current i_{ai} in phase *ai* of the DC-AC converter are shown in Figure 6a–d, respectively.

The experimental results of the WT driving PM synchronous generator system using two sets of PI controllers under middle load (*i.e.*, Δ connection three-phase load of 50Ω) for ω_{r1} = 150 rad/s (n_{r1} = 1500 rpm) are shown in Figure 7. The responses of the rotor speed ω_{r1} (n_{r1}), the step desired DC bus voltage V_d^* and the measured DC bus voltage V_d in output end of the rectifier, the step desired root-mean-square AC 60 Hz line voltage V_{rms}^* and the measured root-mean-square AC 60 Hz line voltage V_{rms} in output end of the inverter, the steady-state desired phase current i_{ai}^* and the measured phase current i_{ai} in phase *ai* of the inverter are shown in Figure 7a–d, respectively.

The experimental results of the WT driving PM synchronous generator system using two sets of PI controllers under heavy load (*i.e.*, Δ connection three-phase load of 18Ω) for ω_{r1} = 209.3 rad/s (n_{r1} = 2000 rpm) are shown in Figure 8. The responses of the rotor speed ω_{r1} (n_{r1}), the step desired DC bus voltage V_d^* and the measured DC bus voltage V_d in output end of the rectifier, the step desired root-mean-square AC 60 Hz line voltage V_{rms}^* and the measured root-mean-square AC 60 Hz line voltage V_{rms} in output end of the inverter, the steady-state desired phase current i_{ai}^* and the measured phase current i_{ai} in phase *ai* of the inverter are shown in Figure 8a–d, respectively.

From the experimental results, sluggish DC bus voltage and AC 60 Hz line voltage tracking are obtained for the PI controlled WT driving PM synchronous generator system due to the weak robustness of the linear controller.

Some experimental results of the WT driving PM synchronous generator system using the two sets of novel recurrent Chebyshev NN control systems are discussed. The experimental results of the WT driving PM synchronous generator system using the novel recurrent Chebyshev NN control system under light load (*i.e.*, Δ connection three-phase load of 100Ω) for ω_{r1} = 78.5 rad/s (n_{r1} = 750 rpm) are shown in Figure 9. The responses of the rotor speed ω_{r1} (n_{r1}), the step desired DC bus voltage V_d^* and the measured DC bus voltage V_d in output end of the rectifier, the step desired root-mean-square AC 60 Hz line voltage V_{rms}^* and the measured root-mean-square AC 60 Hz line voltage V_{rms} in output end of the inverter, the steady-state desired phase current i_{ai}^* and the measured phase current i_{ai} in phase *ai* of the inverter are shown in Figure 9a–d, respectively.

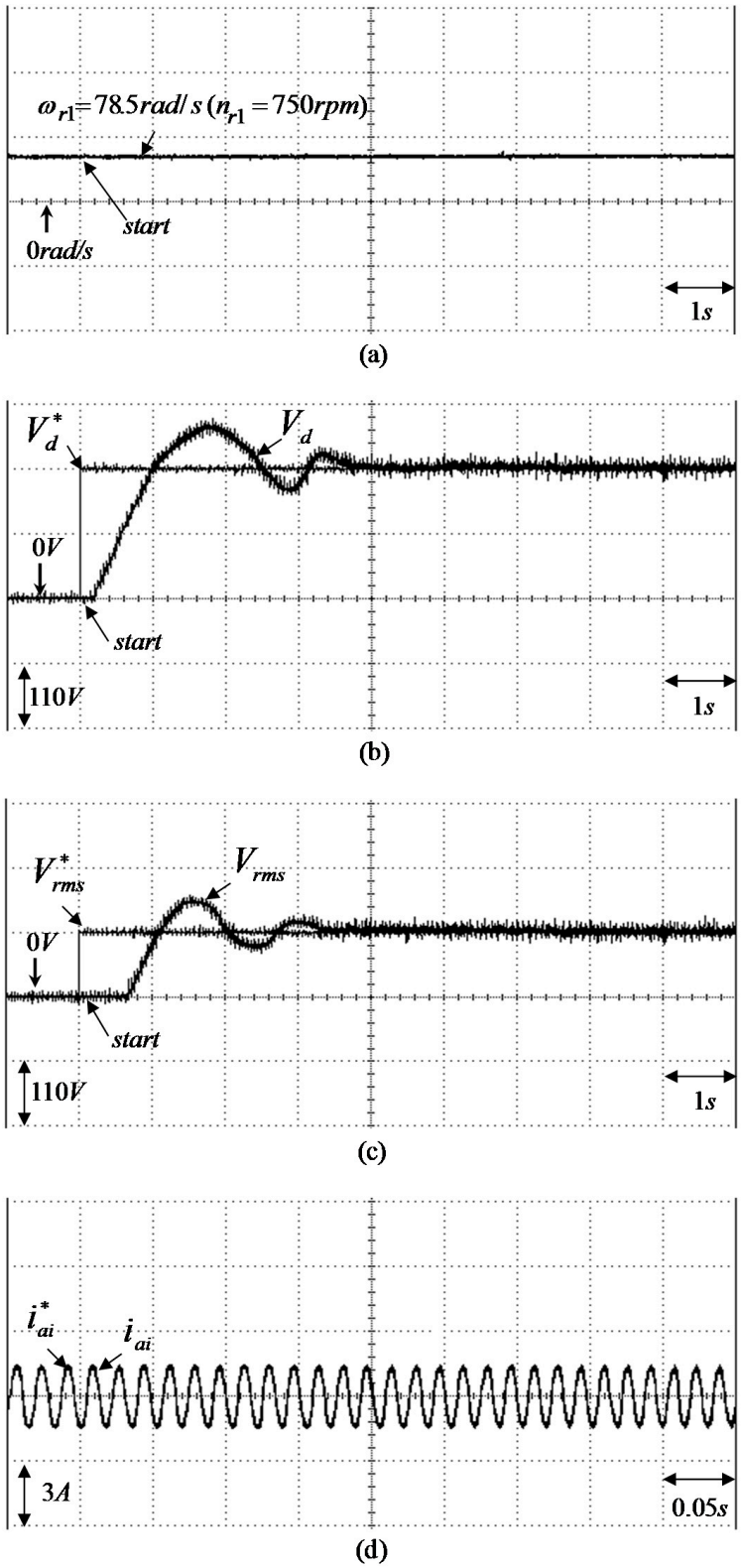

Figure 6. Experimental results of the WT driving PM synchronous generator system using two sets of PI controllers under light load (*i.e.*, Δ connection three-phase load of 100Ω) for ω_{r1} = 78.5 rad/s (n_{r1}= 750 rpm): (**a**) rotor speed $\omega_{r1}(n_{r1})$; (**b**) adjusting response of step desired DC bus voltage V_d^* and measured DC bus voltage V_d in output end of the AC-DC converter; (**c**) adjusting response of step desired root-mean-square AC 60 Hz line voltage V_{rms}^* and measured root-mean-square AC 60 Hz line voltage V_{rms} in output end of the DC-AC converter; (**d**) tracking response of the desired phase current i_{ai}^* and measured phase current i_{ai} in phase *ai* of the DC-AC converter.

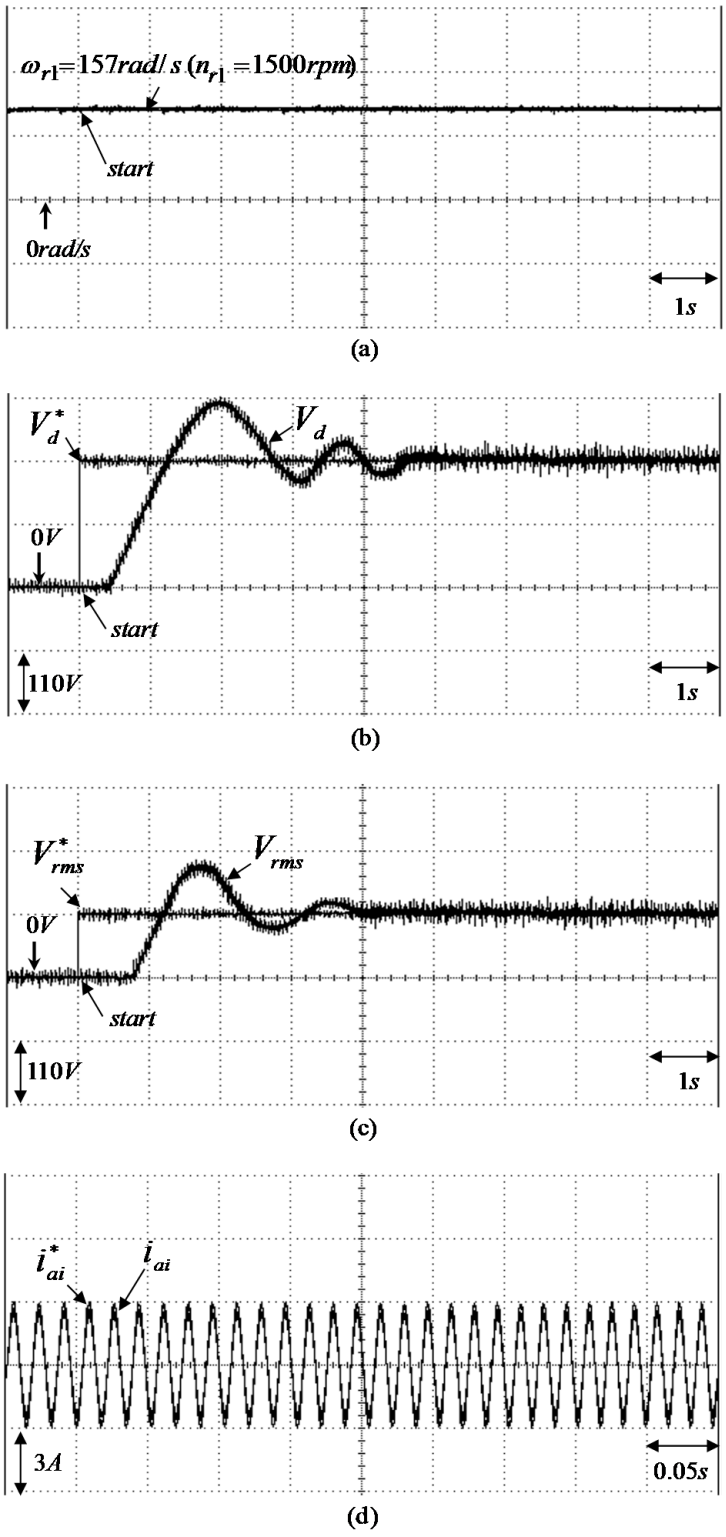

Figure 7. Experimental results of the WT driving PM synchronous generator system using two sets of PI controllers under middle load *(i.e.*, Δ connection three-phase load of 50Ω) for ω_{r1} = 157 rad/s (n_{r1} = 1500 rpm): (**a**) rotor speed $\omega_{r1}(n_{r1})$; (**b**) adjusting response of step desired DC bus voltage V_d^* and measured DC bus voltage V_d in output end of the AC-DC converter; (**c**) adjusting response of step desired root-mean-square AC 60Hz line voltage V_{rms}^* and measured root-mean-square AC 60Hz line voltage V_{rms} in output end of the DC-AC converter; (**d**) tracking response of the desired phase current i_{ai}^* and measured phase current i_{ai} in phase *ai* of the DC-AC converter.

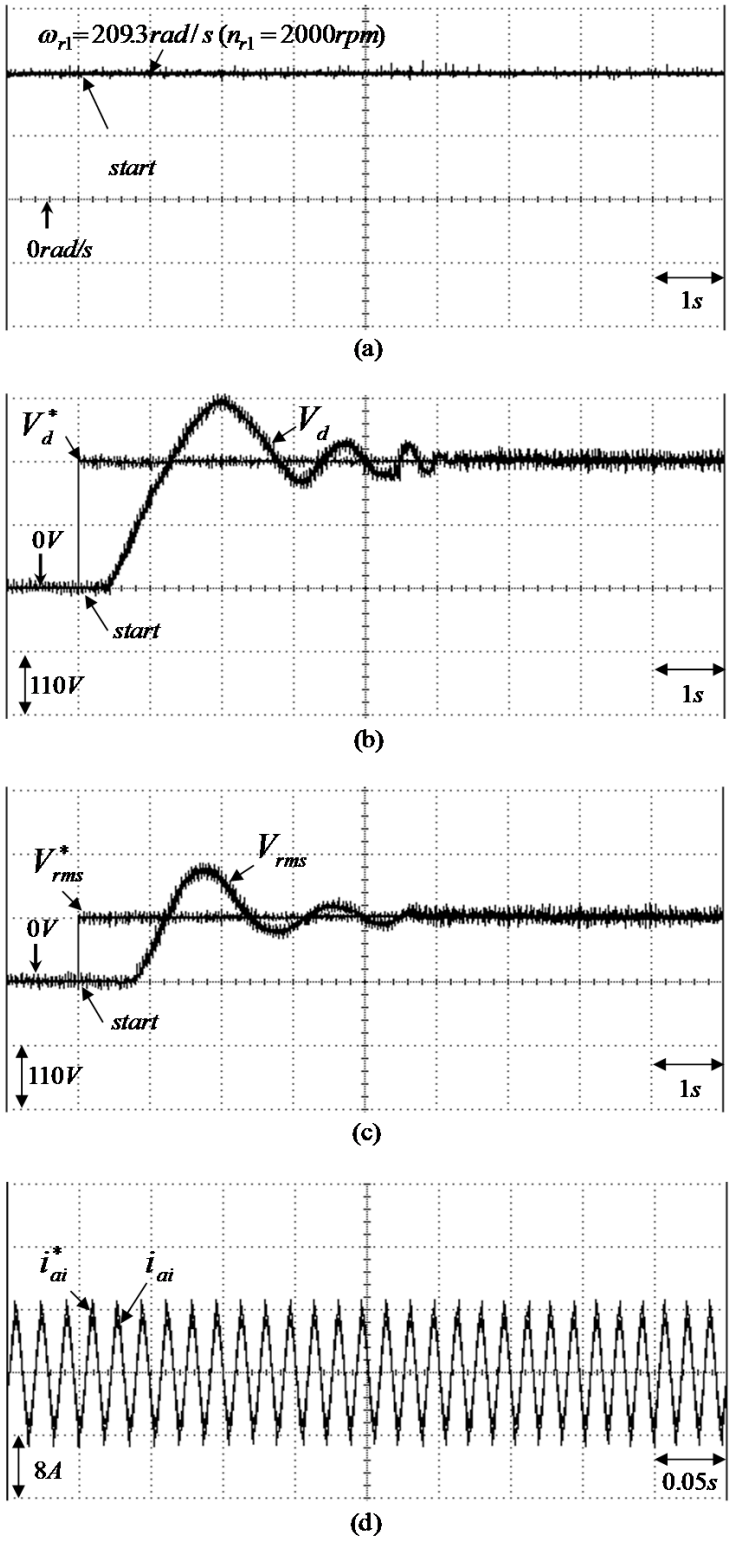

Figure 8. Experimental results of the WT driving PM synchronous generator system using two sets of PI controllers under heavy load (*i.e.*, Δ connection three-phase load of 18Ω) for ω_{r1} = 209.3 rad/s (n_{r1} = 2000 rpm): (**a**) rotor speed $\omega_{r1}(n_{r1})$; (**b**) adjusting response of step desired DC bus voltage V_d^* and measured DC bus voltage V_d in output end of the AC-DC converter; (**c**) adjusting response of step desired root-mean-square AC 60Hz line voltage V_{rms}^* and measured root-mean-square AC 60 Hz line voltage V_{rms} in output end of the DC-AC converter; (**d**) tracking response of the desired phase current i_{ai}^* and measured phase current i_{ai} in phase *ai* of the DC-AC converter.

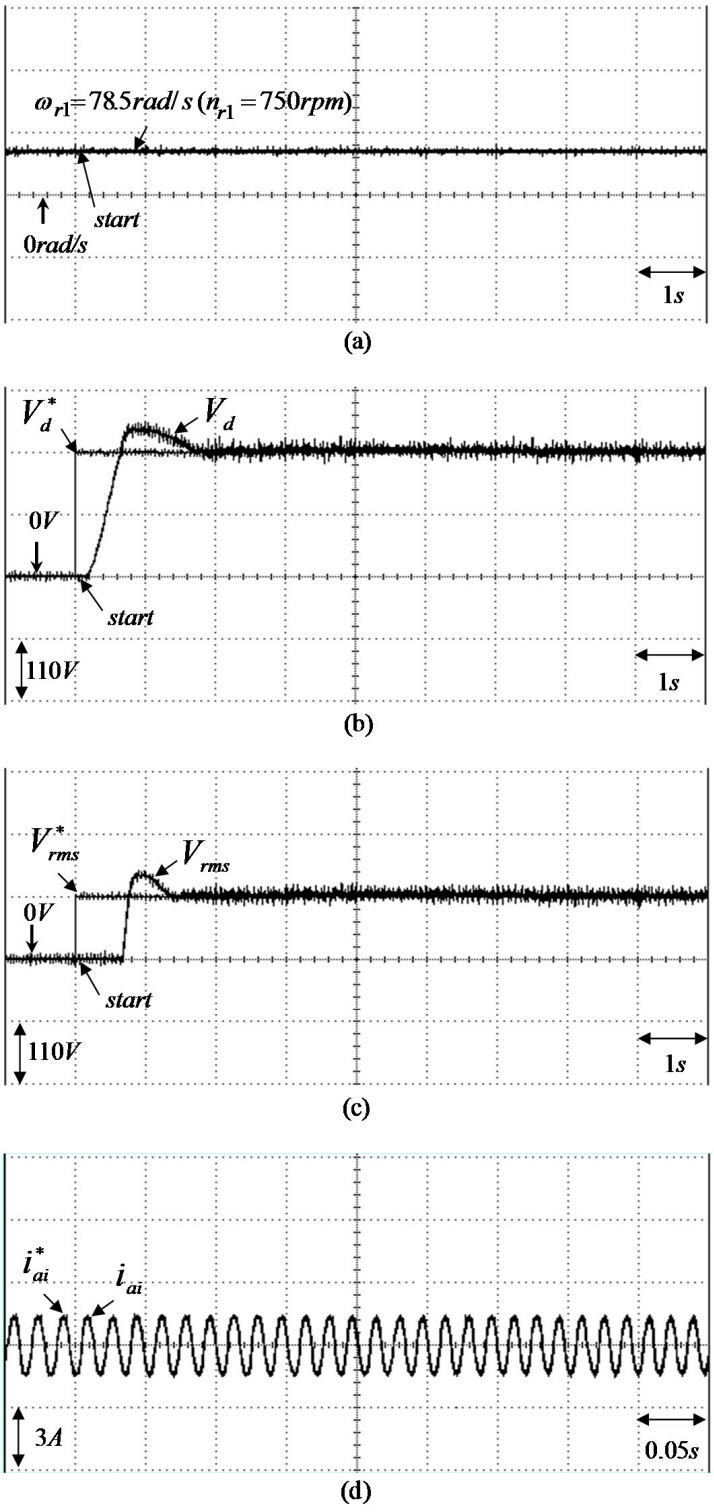

Figure 9. Experimental results of the WTE driving PM synchronous generator system using the two sets of novel recurrent Chebyshev NN control system under light load (*i.e.*, Δ connection three-phase load of 100Ω) for ω_{r1} = 78.5 rad/s (n_{r1} = 750 rpm): (**a**) rotor speed $\omega_{r1}(n_{r1})$; (**b**) adjusting response of step desired DC bus voltage V_d^* and measured DC bus voltage V_d in output end of the AC-DC converter; (**c**) adjusting response of step desired root-mean-square AC 60Hz line voltage V_{rms}^* and measured root-mean-square AC 60 Hz line voltage V_{rms} in output end of the DC-AC converter; (**d**) tracking response of the desired phase current i_{ai}^* and measured phase current i_{ai} in phase *ai* of the DC-AC converter.

The experimental results of the WT driving PM synchronous generator system using the two sets of novel recurrent Chebyshev NN control system under middle load (*i.e.*, Δ connection three-phase load of 50Ω) for ω_{r1} = 150 rad/s (n_{r1} = 1500 rpm) are shown in Figure 10. The responses of the rotor speed ω_{r1} (n_{r1}), the step desired DC bus voltage V_d^* and the measured DC bus voltage V_d in output end of the rectifier, the step desired root-mean-square AC 60 Hz line voltage V_{rms}^* and the measured root-mean-square AC 60 Hz line voltage V_{rms} in output end of the inverter, the steady-state desired phase current i_{ai}^* and the measured phase current i_{ai} in phase *ai* of the DC-AC converter are shown in Figure 10a–d, respectively.

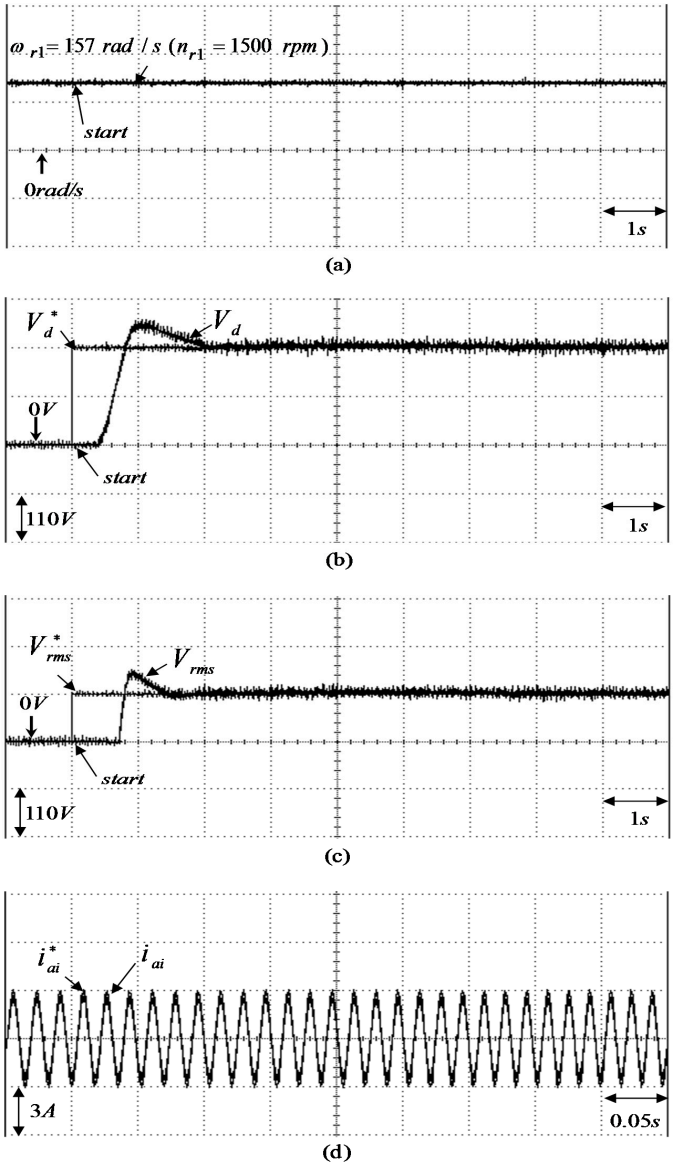

Figure 10. Experimental results of the WT driving PM synchronous generator system using th two sets of novel recurrent Chebyshev NN control system under middle load (*i.e.*, Δ connection three-phase load of 50Ω) for ω_{r1} = 157 rad/s (n_{r1} = 1500 rpm): (**a**) rotor speed $\omega_{r1}(n_{r1})$; (**b**) adjusting response of step desired DC bus voltage V_d^* and measured DC bus voltage V_d in output end of the AC-DC converter; (**c**) adjusting response of step desired root-mean-square AC 60 Hz line voltage V_{rms}^* and measured root-mean-square AC 60 Hz line voltage V_{rms} in output end of the DC-AC converter; (**d**) tracking response of the desired phase current i_{ai}^* and measured phase current i_{ai} in phase *ai* of the DC-AC converter.

The experimental results of the WT driving PM synchronous generator system using the two sets of novel recurrent Chebyshev NN control system under heavy load (*i.e.*, Δ connection three-phase load of 18Ω) for ω_{r1} = 209.3 rad/s (n_{r1} = 2000 rpm) are shown in Figure 11. The responses of the rotor speed ω_{r1} (n_{r1}), the step desired DC bus voltage V_d^* and the measured DC bus voltage V_d in output end of the rectifier, the step desired root-mean-square AC 60 Hz line voltage V_{rms}^* and the measured root-mean-square AC 60 Hz line voltage V_{rms} in output end of the inverter, the steady-state desired phase current i_{ai}^* and the measured phase current i_{ai} in phase *ai* of the DC-AC converter are shown in Figure 11a–d, respectively.

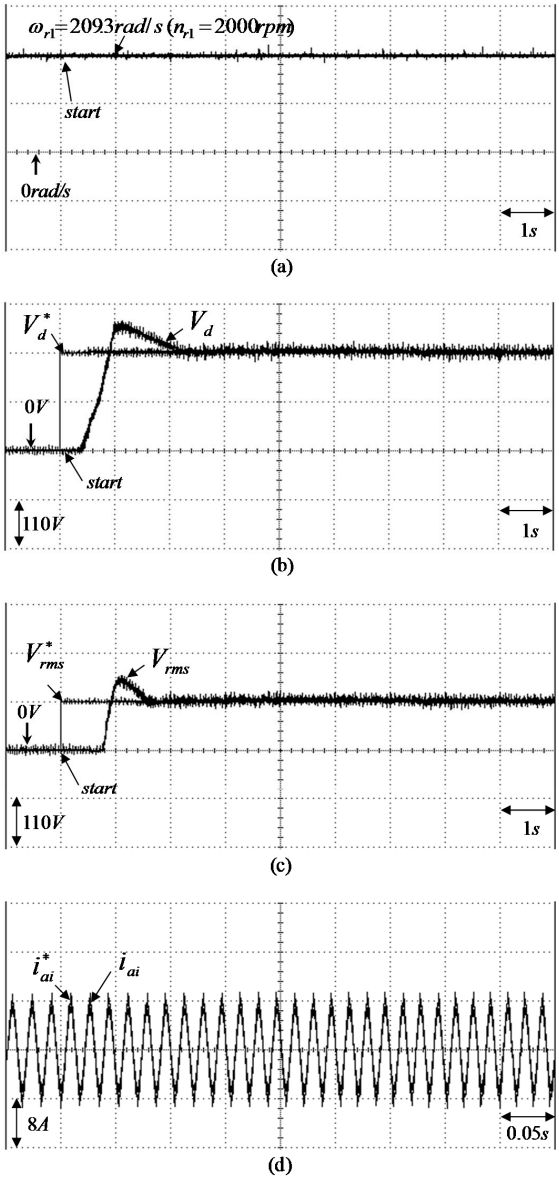

Figure 11. Experimental results of the WT driving PM synchronous generator system using the two sets of novel recurrent Chebyshev NN control system under heavy load (*i.e.*, Δ connection three-phase load of 18Ω) for ω_{r1} = 209.3 rad/s (n_{r1} = 2000 rpm): (**a**) rotor speed $\omega_{r1}(n_{r1})$; (**b**) adjusting response of step desired DC bus voltage V_d^* and measured DC bus voltage V_d in output end of the AC-DC converter; (**c**) adjusting response of step desired root-mean-square AC 60 Hz line voltage V_{rms}^* and measured root-mean-square AC 60 Hz line voltage V_{rms} in output end of the DC-AC converter; (**d**) tracking response of the desired phase current i_{ai}^* and measured phase current i_{ai} in phase *ai* of the DC-AC converter.

Moreover, compared with the PI control method, the proposed novel recurrent Chebyshev NN control method has a superior tracking and a good improvement owing to on-line training of the novel recurrent Chebyshev NN.

Since this study is dealing with an isolated system with maximum power control, the block diagram of the DC bus power with maximum power control is also the same as Figure 3 except V_d^* is replaced by P_d^* and V_d is replaced by P_d. The experimental results for the varying wind turbine speed with maximum DC bus power of the PM synchronous generator system are provided. The experimental results of the novel recurrent Chebyshev NN control system controlled PM synchronous generator system at the condition of step changes of rotor speed, *i.e.*, 350, 750 and 1500 rpm, for the command tracking of are shown in Figure 12. The responses of the rotor speed ω_{r1} (n_{r1}), the measured DC bus voltage V_d, the measured DC bus current I_d, the reference DC bus power P_d^* and DC bus power P_d are shown in Figure 12a–d, respectively. From the experimental results, favorable DC bus power tracking response can be achieved by using the novel recurrent Chebyshev NN control system.

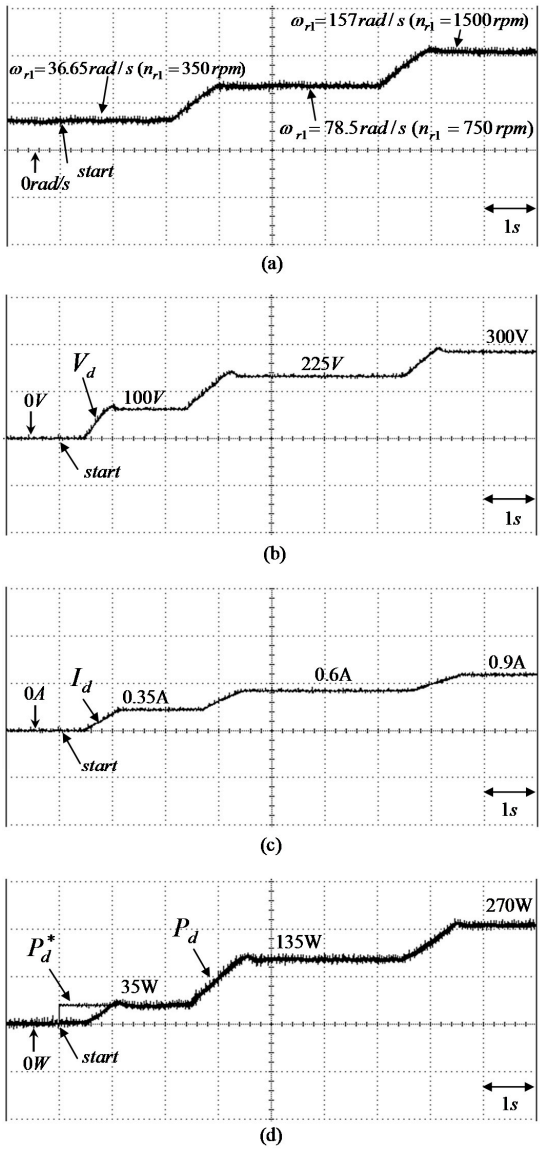

Figure 12. Experimental results of the WT driving PM synchronous generator system using the novel recurrent Chebyshev NN control system at step-command changing of rotor speed: (**a**) rotor speed $\omega_{r1}(n_{r1})$; (**b**) response of measured DC bus voltage V_d; (**c**) response of measured DC bus current I_d; (**d**) response of reference DC bus power P_d^* and DC bus power P_d.

6. Conclusions

This paper demonstrated the implementation of the novel recurrent Chebyshev NN control system to regulate both the DC bus voltage of the AC-DC converter provided by PM synchronous generator system and AC line voltage of the DC-AC converter in order to supply for smart grid power application. The control performance of the proposed novel recurrent Chebyshev NN control system is robust with regard to different operating conditions of the PM synchronous generator system. The major contributions of this paper are: (1) the successful development of the PM synchronous generator system for smart grid power application through a AC-DC converter and a DC-AC converter; (2) the successful development of the novel recurrent Chebyshev NN control system in which the Lyapunov stability theorem is used in online tuning of the parameters; (3) the successful development of an online training methodology with variable learning rate for the novel recurrent Chebyshev NN control system; (4) the successful application of the two sets of novel recurrent Chebyshev NN control systems in the PM synchronous generator system to regulate the DC bus voltage of the AC-DC converter and the AC line voltage of the DC-AC converter. Finally, control performance of the proposed novel recurrent Chebyshev NN control system shown in experimental results is superior to the PI controller for the PM synchronous generator system directly driven by wind turbine through AC-DC converter and DC-AC converter for smart grid power application.

Acknowledgments: The author would like to acknowledge the financial support of the Ministry of Science and Technology in Taiwan through its grant MOST 103-2221-E-239-016.

Conflicts of Interest: The author declares no conflict of interest.

References

1. Tan, K.; Islam, S. Optimum control strategies in energy conversion of PMSG wind turbine system without mechanical sensors. *IEEE Trans. Energy Convers.* **2004**, *19*, 392–400. [CrossRef]
2. Andersen, G.K.; Klumpner, C.; Kjaer, S.B.; Blaabjerg, F. A new green power inverter for fuel cells. In Proceedings of the IEEE 33rd Annual Power Electron, Specialists Conference, Cairns, Queensland, Australia, 23–27 June 2002; pp. 727–733.
3. Kim, Y.; Chung, I.; Moon, S. Tuning of the PI controller parameters of a PMSG wind turbine to improve control performance under various wind speeds. *Energies* **2015**, *8*, 1406–1425. [CrossRef]
4. Lubosny, Z. *Wind Turbine Operation in Electric Power Systems*; Springer: Berlin, Germany, 2003.
5. Ackermann, T. *Wind Power in Power Systems*; John Wiley & Sons: New York, NY, USA, 2005.
6. Karrari, M.; Rosehart, W.; Malik, Q.P. Comprehensive control strategy for a variable speed cage machine wind generation unit. *IEEE Trans. Energy Convers.* **2005**, *20*, 415–423. [CrossRef]
7. Chinchilla, M.; Arnaltes, S.; Burgos, I.C. Control of permanent magnet Generators applied to variable-speed wind-energy systems connected to the grid. *IEEE Trans. Energy Convers.* **2006**, *21*, 130–135. [CrossRef]
8. Eminoglu, U.; Ayasun, S. Modeling and design optimization of variable-speed wind turbine systems. *Energies* **2014**, *7*, 402–419. [CrossRef]
9. Lin, C.H. Novel modified Elman neural network control for PMSG system based on wind turbine emulator. *Math. Probl. Eng.* **2013**, *2013*, 753756. [CrossRef]
10. Lin, C.H. Recurrent modified Elman neural network control of PM synchronous generator system using wind turbine emulator of PM synchronous servo motor drive. *Int. J. Electr. Power Energy Syst.* **2013**, *52*, 143–160. [CrossRef]
11. Simoes, M.G.; Bose, B.K.; Spiegel, R.J. Design and performance evaluation of a fuzzy-logic-based variable-speed wind generation system. *IEEE Trans. Ind. Appl.* **1997**, *33*, 956–965. [CrossRef]
12. Zeng, Q.; Chang, L.; Shao, R. Fuzzy-logic-based maximum power point tracking strategy for PMSG variable-speed wind turbine generation systems. In Proceedings of the 21st Canadian Conference Electric Computer Engineering, Niagara Falls, ON, Canada, 4–7 May 2008; pp. 405–409.
13. Uehara, A.; Senjyu, T.; Yona, A.; Funabashi, T.; Kim, C.H. A fuzzy-logic based output power smoothing method of WECS with permanent magnet synchronous generator using inertia of wind turbine. *J. Int. Counc. Electr. Eng.* **2011**, *1*, 309–316. [CrossRef]

14. Amimeur, H.; Aouzellag, D.; Abdessemed, R.; Ghedamsi, K. Sliding mode control of a dual-stator induction generator for wind energy conversion systems. *Int. J. Electr. Power Energy Syst.* **2012**, *42*, 60–70. [CrossRef]
15. Lin, W.M.; Hong, C.H.; Lee, M.R.; Huang, C.H.; Huang, C.C.; Wu, B.L. Fuzzy-sliding mode based control for PMSM maximum wind energy capture with compensated pitch angle. In Proceedings of the 2010 International Symposium on Computer, Communication, Control and Automation, Tainan, Taiwan, 5–7 May 2010; pp. 397–400.
16. Lin, W.M.; Hong, C.M.; Ou, T.C.; Chiu, T.M. Hybrid intelligent control of PMSG wind generation system using pitch angle control with RBFN. *Energy Convers. Manag.* **2011**, *52*, 1244–1251. [CrossRef]
17. Lin, W.M.; Hong, C.M. A new Elman neural network-based control algorithm for adjustable-pitch variable-speed wind-energy conversion systems. *IEEE Trans. Power Electron. 201* **2011**, *26*, 473–481. [CrossRef]
18. Lin, C.H. Recurrent modified Elman neural network control of permanent magnet synchronous generator system based on wind turbine emulator. *J. Renew. Sustain. Energy* **2013**, *5*, 053103. [CrossRef]
19. Haykin, S. *Neural Networks*; Maxwell Macmillan: Ottawa, ON, Canada, 1994; pp. 124–128.
20. Sastry, P.S.; Santharam, G.; Unnikrishnan, K.P. Memory neural networks for identification and control of dynamical systems. *IEEE Trans. Neural Netw.* **1994**, *5*, 306–319. [CrossRef] [PubMed]
21. Grino, R.; Cembrano, G.; Torras, C. Nonlinear system identification using additive dynamic neural networks—Two on-line approaches. *IEEE Trans. Circuits Syst. I Fundam. Theory Appl.* **2000**, *47*, 150–165. [CrossRef]
22. Pao, Y.H. *Adaptive Pattern Recognition and Neural Networks*; Addison-Wesley: Reading, MA, USA, 1989.
23. Pao, Y.H.; Philips, S.M. The functional link net and learning optimal control. *Neurocomputing* **1995**, *9*, 149–164. [CrossRef]
24. Patra, J.C.; Pal, R.N.; Chatterji, B.N.; Panda, G. Identification of nonlinear dynamic systems using functional link artificial neural networks. *IEEE Trans. Syst. Man Cybern. B* **1999**, *29*, 254–262. [CrossRef] [PubMed]
25. Dehuri, S.; Cho, S.-B. A comprehensive survey on functional link neural networks and an adaptive PSOBP learning for CFLNN. *Neural Comput. Appl.* **2010**, *9*, 187–205. [CrossRef]
26. Ueda, N.N. Pattern classification with Chebyshev neural networks. *Int. J. Neural Netw.* **1992**, *3*, 23–31.
27. Lee, T.T.; Jeng, J.T. The Chebyshev polynomial-based unified model neural networks for functional approximation. *IEEE Trans. Syst. Man Cybern. B* **1998**, *28*, 925–935.
28. Moller, M.F. A scaled conjugate gradient algorithm for fast supervised learning. *Neural Netw.* **1993**, *6*, 525–533. [CrossRef]
29. Battiti, R. First- and second-order methods for learning: Between steepest descent and Newton's method,". *Neural Comput.* **1992**, *4*, 141–166.
30. Charalambous, C. Conjugate gradient algorithm for efficient training of artificial neural networks. *Proc. Inst. Electr. Eng. G* **1992**, *139*, 301–310. [CrossRef]
31. Hagan, M.T.; Menhaj, M.B. Training feedforward networks with Marquardt algorithm. *IEEE Trans. Neural Netw.* **1994**, *5*, 989–993. [CrossRef] [PubMed]
32. Madyastha, R.K.; Aazhang, B. An algorithm for training multilayer perceptrons for data classification and function interpolation. *IEEE Trans. Circuits Syst. I* **1994**, *41*, 866–875. [CrossRef]
33. Brdys, M.A.; Kulawski, G.J. Dynamic neural controllers for induction motor. *IEEE Trans Neural Netw.* **1999**, *10*, 340–355. [CrossRef] [PubMed]
34. Li, X.D.; Ho, J.K.L.; Chow, T.W.S. Approximation of dynamical time-variant systems by continuous-time recurrent neural networks. *IEEE Trans Circuits Syst II* **2005**, *52*, 656–660.
35. Hamrouni, N.; Jraidi, M.; Cherif, A. New control strategy for 2-stage grid-connected photovoltaic system. *Renew. Energy* **2008**, *33*, 2212–2221. [CrossRef]
36. Wang, L.X. *Adaptive Fuzzy Systems and Control: Design and Stability Analysis*; Prentice-Hall: New York, NY, USA, 1994.
37. Astrom, J.; Wittenmark, B. *Adaptive Control*; Addison-Wesley: New York, NY, USA, 1995.